Hypertriton lifetime

D. Gazda,[1,*] A. Pérez-Obiol,[2,†] E. Friedman,[3] and A. Gal[3]
[1]*Nuclear Physics Institute, 25068 Řež, Czech Republic*
[2]*Barcelona Supercomputing Center, 08034 Barcelona, Spain*
[3]*Racah Institute of Physics, The Hebrew University, 9190401 Jerusalem, Israel*

(Received 4 October 2023; accepted 2 January 2024; published 6 February 2024)

Over the last decade, conflicting values of the hypertriton ${}^{3}_{\Lambda}$H lifetime $\tau({}^{3}_{\Lambda}\mathrm{H})$ were extracted from relativistic heavy-ion (RHI) collision experiments, ranging from values compatible with the free-Λ lifetime τ_Λ—as expected naively for a very weakly bound Λ in ${}^{3}_{\Lambda}$H—to lifetimes as short as $\tau({}^{3}_{\Lambda}\mathrm{H}) \approx (0.4\text{–}0.7)\,\tau_\Lambda$. In a recent work [Phys. Lett. B **811**, 135916 (2020)] we studied this ${}^{3}_{\Lambda}$H lifetime puzzle theoretically using realistic three-body ${}^{3}_{\Lambda}$H and ^{3}He wave functions computed within the *ab initio* no-core shell model approach with interactions derived from chiral effective field theory to calculate the partial decay rate $\Gamma({}^{3}_{\Lambda}\mathrm{H} \to {}^{3}\mathrm{He} + \pi^-)$. Significant but opposing contributions were found from ΣNN admixtures in ${}^{3}_{\Lambda}$H and from π^--^{3}He final-state interaction. In particular, $\tau({}^{3}_{\Lambda}\mathrm{H})$ was found to be strongly correlated with the Λ separation energy B_Λ in ${}^{3}_{\Lambda}$H, the value of which is rather poorly known experimentally and, in addition, is known to suffer from sizable theoretical uncertainties inherent in the employed nuclear and hypernuclear interaction models. In the present work we find that these uncertainties propagate into $\tau({}^{3}_{\Lambda}\mathrm{H})$, and thus limit considerably the theoretical precision of its computed value. Although none of the conflicting RHI measured $\tau({}^{3}_{\Lambda}\mathrm{H})$ values can be excluded, but rather can be attributed to a poor knowledge of B_Λ, we note the good agreement between the lifetime value $\tau({}^{3}_{\Lambda}\mathrm{H}) = 242(28)$ ps computed at the lowest value $B_\Lambda = 66$ keV reached by us and the very recent ALICE measured lifetime value $\tau^{\mathrm{ALICE}}({}^{3}_{\Lambda}\mathrm{H}) = 253(11)(6)$ ps associated with the ALICE measured B_Λ value $B_\Lambda^{\mathrm{ALICE}} = 102(63)(67)$ keV [S. Acharya *et al.* (ALICE Collaboration), Phys. Rev. Lett. **131**, 102302 (2023)].

DOI: 10.1103/PhysRevC.109.024001

I. INTRODUCTION

The hypertriton (${}^{3}_{\Lambda}$H) is the lightest bound hypernucleus, with isospin $T = 0$ and spin-parity $J^P = \frac{1}{2}^+$ [1]. Together with other s-shell light Λ hypernuclei, ${}^{4}_{\Lambda}$H–${}^{4}_{\Lambda}$He and ${}^{5}_{\Lambda}$He, it provides useful constraints on the poorly known YN and YNN interactions [2] which are tested in heavier Λ hypernuclei in the context of hyperon composition of dense baryonic matter realized perhaps in the cores of neutron stars [3–5]. Owing to the extremely small Λ separation energy in ${}^{3}_{\Lambda}$H, $B_\Lambda = 164(43)$ keV [6], the structure of ${}^{3}_{\Lambda}$H should resemble to a good approximation that of a Λ bound loosely to a deuteron (^{2}H) core with a mean distance of ≈ 10 fm. The lifetime of such a loosely bound system is expected to be comparable to the lifetime of the free Λ, $\tau_\Lambda = 263(2)$ ps [7], the decay of which to 99.7% is driven by the $\Lambda \to N\pi$ nonleptonic weak transitions.

Yet, while the most recent ALICE Collaboration's measurement [8] reports a $\tau({}^{3}_{\Lambda}\mathrm{H})$ closely agreeing with the free-Λ lifetime τ_Λ, $\tau^{\mathrm{ALICE}}({}^{3}_{\Lambda}\mathrm{H}) = 253(11)(6)$ ps $\approx 0.96\tau_\Lambda$, considerably shorter values $\tau({}^{3}_{\Lambda}\mathrm{H}) \approx (0.5\text{–}0.7)\tau_\Lambda$ were extracted in recent RHI collision experiments by the STAR [9] and HypHI [10] Collaborations. We note that the latest STAR Collaboration's measurement [11], reporting a value of $\tau^{\mathrm{STAR}}({}^{3}_{\Lambda}\mathrm{H}) = 221(15)(19)$ ps, comes close within its experimental uncertainties to τ_Λ, but its central value is still about 15% shorter. It is to be noted that a similarly large spread of $\tau({}^{3}_{\Lambda}\mathrm{H})$ values, although with larger uncertainties, had been reported in older nuclear-emulsion and helium bubble-chamber (BC) hypernuclear measurements [12–17], as shown in Fig. 1. Also shown in the figure are the $\tau({}^{3}_{\Lambda}\mathrm{H})$ values from recent RHI collision experiments [8–11,18–20], together with representative (post-1997) theoretical calculations [21–24].

Several theoretical approaches with varying degree of sophistication have been employed to study the decay of the hypertriton [21–24,26,27] by calculating π^- decay rates and using the $\Delta T = \frac{1}{2}$ rule (see Sec. II A) to add the corresponding π^0 decay rates. In the first calculation marked in Fig. 1, a value of $\tau({}^{3}_{\Lambda}\mathrm{H})$ shorter by only 6% than τ_Λ was obtained in a full Λnp Faddeev calculation accounting for all ${}^{3}_{\Lambda}$H two-, three-, and four-body π^- decay channels (^{3}He π^-, ^{2}H $p\pi^-$, and $npp\pi^-$, all with plane-wave pions). However, the Nijmegen SC89 YN interaction [28] applied there to construct the ${}^{3}_{\Lambda}$H wave function was shown to be problematic in hypernuclei, starting at $A = 4$ [29]. In the second calculation [22], a value of $\tau({}^{3}_{\Lambda}\mathrm{H}) \approx 0.8\,\tau_\Lambda$ was obtained within the closure approximation using three-body ${}^{3}_{\Lambda}$H wave functions generated from Λnp Faddeev equations. Here, half of the $\approx 20\%$ reduction in $\tau({}^{3}_{\Lambda}\mathrm{H})$ resulted from the attractive final-state interaction (FSI) of the outgoing pion. While a fixed value of $B_\Lambda \approx 135$ keV was used in these two $\tau({}^{3}_{\Lambda}\mathrm{H})$ calculations, a range of B_Λ values was tested in the next two

*Corresponding author: gazda@ujf.cas.cz
†axel.perezobiol@bsc.es

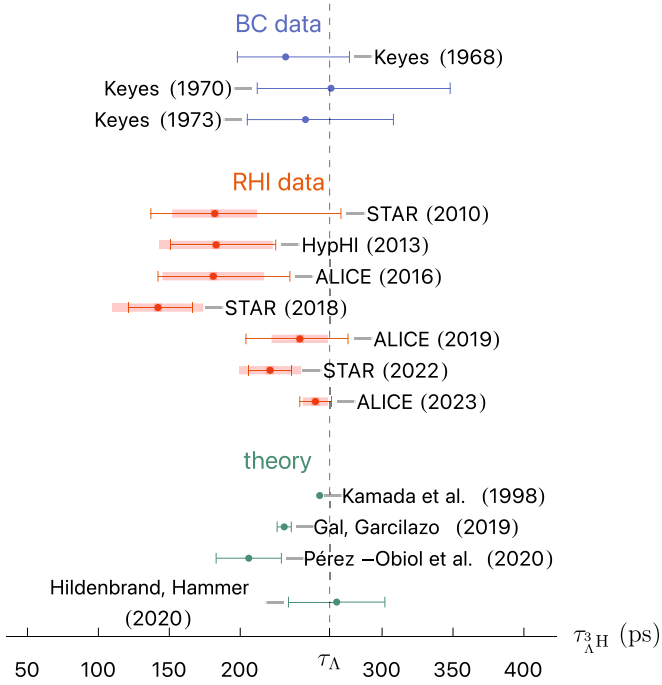

FIG. 1. $^3_\Lambda$H lifetime values $\tau(^3_\Lambda\mathrm{H})$ obtained in selected [25] past nuclear BC [14,15,17] and recent RHI collision [8–11,18–20] experiments, together with a few (post-1997) microscopic calculations [21–24]; see text. Error bars and shaded areas indicate the measurement statistical and systematical errors, respectively, as well as the estimated theoretical uncertainties (if available). The vertical dashed line corresponds to the free-Λ lifetime value $\tau_\Lambda = 263(2)$ ps [7].

calculations. The $\tau(^3_\Lambda\mathrm{H})$ intervals shown in the figure for these calculations [23,24] correspond to the central value $B_\Lambda =$ 102 keV reported by the most recent ALICE measurement [8]. In the third calculation [23] we established significant but opposing contributions from pionic FSI and ΣNN admixtures in $^3_\Lambda$H, by using chiral effective field theory (χEFT) nuclear and hypernuclear interactions to obtain realistic ^{3}He and $^3_\Lambda$H 3-body wave functions within an *ab initio* no-core shell model (NCSM) approach for evaluating the two-body $^3_\Lambda\mathrm{H} \to {}^3\mathrm{He} + \pi^-$ partial decay rate. The known branching ratio $\Gamma(^3_\Lambda\mathrm{H} \to {}^3\mathrm{He} + \pi^-)/\Gamma(^3_\Lambda\mathrm{H} \to$ all π^- channels) was then utilized to compute the inclusive π^- decay rate. Finally, $\tau(^3_\Lambda\mathrm{H}) \approx \tau_\Lambda$ was obtained in the last calculation displayed in the figure [24], with relatively large uncertainties of $\gtrsim$15%, by applying pionless effective field theory (EFT) and reducing the three-body $^3_\Lambda$H and ^{3}H, ^{3}He systems to loosely bound ^{2}H-Λ and ^{2}H-N two-body systems, respectively. Adding pionic FSI was found in a very recent application of this pionless EFT work to enhance the $^3_\Lambda$H decay rate by about 18% [30]. The central value of the $\tau(^3_\Lambda\mathrm{H})$ interval in Fig. 1 moves then from about τ_Λ down to 84% of it, namely to 221 ps, in rough agreement with our result [23].

In the present work, we extend and provide full details of our recent $^3_\Lambda$H lifetime calculation [23]. More specifically, we employ precise realistic three-body $^3_\Lambda$H and ^{3}He wave functions to evaluate the $^3_\Lambda$H two-body π^- partial decay rate and relate it to the inclusive pionic $^3_\Lambda$H decay rate and $\tau(^3_\Lambda\mathrm{H})$. We account for the distortion of the outgoing π^- wave due to realistic π^--^{3}He interaction and take into account contributions from $\Sigma \to N\pi$ transitions, resulting from ΣNN admixtures in the $^3_\Lambda$H wave function. The main focus of the present work, however, is to explore the theoretical precision of calculating $\Gamma(^3_\Lambda\mathrm{H} \to {}^3\mathrm{He} + \pi^-)$, and thereby $\tau(^3_\Lambda\mathrm{H})$, due to systematic model uncertainties in the YN and $NN + NNN$ interactions. For this purpose we employ four versions of the LO YN interaction regularized at $\Lambda_{YN} = 550,\ 600,\ 650$, and 700 MeV, together with the NNLO$_{\mathrm{sim}}$ family of 42 nuclear interactions.

The paper is organized as follows: In Sec. II we present the formalism to calculate the hypertriton decay rate and lifetime. In particular, in Sec. II A we elaborate on our approach to relate $\tau(^3_\Lambda\mathrm{H})$ to the partial two-body π^- decay rate $\Gamma(^3_\Lambda\mathrm{H} \to {}^3\mathrm{He} + \pi^-)$ introduced in Sec. II B. This partial decay rate is calculated starting from an effective weak-decay operator constructed in Sec. II C and evaluating its matrix elements between π^- (Sec. II D), $^3_\Lambda$H and ^{3}He three-body wave functions (Sec. II E) generated within the NCSM approach using realistic YN and $NN + NNN$ interactions from χEFT described in Sec. II F. In Sec. III, results for the two-body $^3_\Lambda\mathrm{H} \to {}^3\mathrm{He} + \pi^-$ decay rate are presented in Sec. III A, identifying its dominant contributions in Sec. III B and studying in Sec. III C its dependence on the $^3_\Lambda$H Λ separation energy B_Λ. In Sec. III D we quantify the precision limits in predicting theoretically $\Gamma(^3_\Lambda\mathrm{H} \to {}^3\mathrm{He} + \pi^-)$, arising from the uncertainties in the nuclear and hypernuclear three-body wave functions. In Sec. III E, we present and discuss results for the hypertriton lifetime, particularly in light of recent $\tau(^3_\Lambda\mathrm{H})$ measurements. Our main findings are summarized in Sec. IV.

II. METHOD

A. Hypertriton decay

The main decay channels which contribute to the total decay rate rate of the hypertriton are the mesonic (nonleptonic) decay modes due to the weak-interaction $\Lambda \to N\pi$ transitions:

$$\begin{aligned} &^3_\Lambda\mathrm{H} \to {}^3\mathrm{He} + \pi^-, && ^3_\Lambda\mathrm{H} \to {}^3\mathrm{H} + \pi^0, \\ &^3_\Lambda\mathrm{H} \to {}^2\mathrm{H} + p + \pi^-, && ^3_\Lambda\mathrm{H} \to {}^2\mathrm{H} + n + \pi^0, \\ &^3_\Lambda\mathrm{H} \to p + p + n + \pi^-, && ^3_\Lambda\mathrm{H} \to n + n + p + \pi^0. \end{aligned} \tag{1}$$

This is in contrast with heavier hypernuclei where the mesonic decays are Pauli blocked. In (1), only the four-body deuteron-breakup channels are heavily suppressed due to the limited phase space [21]. Apart from the mesonic decays, there is also the nonmesonic decay branch of $^3_\Lambda$H due to $\Lambda N \to NN$:

$$\begin{aligned} &^3_\Lambda\mathrm{H} \to {}^2\mathrm{H} + n, \\ &^3_\Lambda\mathrm{H} \to n + n + p. \end{aligned} \tag{2}$$

The nonmesonic modes, while being the major contributors in the decays of heavy hypernuclei, are known to play a very small role in $^3_\Lambda$H [26,31,32].

The $^3_\Lambda$H partial decay rates corresponding to the charged and neutral pion channels listed in (1) are not independent. Since for the experimental ratio

$\Gamma(\Lambda \to n\pi^0)/\Gamma(\Lambda \to p\pi^-) \approx 0.5$ holds to a good precision, the isospin $T = 0 \to \frac{3}{2}$ ($\Delta T = \frac{3}{2}$) components of the $\Lambda \to p\pi^-, n\pi^0$ amplitudes must be negligible in comparison with the $\Delta T = \frac{1}{2}$ amplitudes. This is known as the "$\Delta T = \frac{1}{2}$ rule" which implies that the transition operators satisfy $\hat{O}_{\Lambda\to p\pi^-} = \sqrt{2}\,\hat{O}_{\Lambda\to n\pi^0}$ and thus relates the charged and neutral pionic rates by $\Gamma_{\pi^-} = 2\,\Gamma_{\pi^0}$. In addition, the measured world-average BC branching ratio $R_3 \equiv \Gamma({}^3_\Lambda\mathrm{H} \to {}^3\mathrm{He} + \pi^-)/\Gamma_{\pi^-}({}^3_\Lambda\mathrm{H}) = 0.35(4)$ [17] can be used to relate the inclusive π^- rate $\Gamma_{\pi^-}({}^3_\Lambda\mathrm{H})$ with the two-body π^- rate $\Gamma^{^3\mathrm{He}} = \Gamma({}^3_\Lambda\mathrm{H} \to {}^3\mathrm{He} + \pi^-)$.

To summarize, in this work we employ the following strategy to evaluate the ${}^3_\Lambda$H lifetime: (i) Use the branching ratio R_3 to get the inclusive π^- rate from the two-body π^- rate $\Gamma({}^3_\Lambda\mathrm{H} \to {}^3\mathrm{He} + \pi^-)$ as

$$\begin{aligned}\Gamma_{\pi^-}({}^3_\Lambda\mathrm{H}) &= \Gamma\big({}^3_\Lambda\mathrm{H} \to {}^3\mathrm{He} + \pi^-\big) \\ &\quad + \Gamma\big({}^3_\Lambda\mathrm{H} \to {}^2\mathrm{H} + p + \pi^-\big) \\ &\quad + \Gamma\big({}^3_\Lambda\mathrm{H} \to n + p + p + \pi^-\big) \\ &= \frac{1}{R_3}\Gamma\big({}^3_\Lambda\mathrm{H} \to {}^3\mathrm{He} + \pi^-\big). \end{aligned} \tag{3}$$

(ii) Include the π^0 decay channels by employing the empirical $\Delta T = \frac{1}{2}$ rule

$$\Gamma_\pi = \Gamma_{\pi^-} + \Gamma_{\pi^0} = \tfrac{3}{2}\,\Gamma_{\pi^-} = \tau_\pi^{-1}\big({}^3_\Lambda\mathrm{H}\big). \tag{4}$$

(iii) Account for the nonmesonic $\Lambda N \to NN$ and pionic true-absorption $\pi + NN \to NN$ contributions through an increase of the ${}^3_\Lambda$H decay rate by 1.5% and 0.8% [26,31,32], respectively; $\tau({}^3_\Lambda\mathrm{H}) = 0.978\,\tau_\pi({}^3_\Lambda\mathrm{H})$.

B. Two-body decay rate $\Gamma({}^3_\Lambda\mathrm{H} \to {}^3\mathrm{He} + \pi^-)$

We follow Ref. [21] which relates the ${}^3_\Lambda$H two-body π^- decay rate $\Gamma({}^3_\Lambda\mathrm{H} \to {}^3\mathrm{He} + \pi^-)$ in the total momentum zero frame to the $\Lambda \to N\pi^-$ free-Λ weak-decay vertex operator $\hat{O}$ as

$$\begin{aligned}\Gamma^{^3\mathrm{He}} &= \frac{1}{2}\sum_{m_{^3_\Lambda\mathrm{H}}}\sum_{m_{^3\mathrm{He}}}\int \mathrm{d}^3p_{^3\mathrm{He}}\,\frac{\mathrm{d}^3p_\pi}{8\pi^2E_\pi} \\ &\quad\times\left|\sqrt{3}\left\langle\Psi_{^3\mathrm{He};\vec{p}_{^3\mathrm{He}},m_{^3\mathrm{He}}}\phi_{\pi;\vec{p}_\pi}\middle|\hat{O}\middle|\Psi_{^3_\Lambda\mathrm{H};m_{^3_\Lambda\mathrm{H}}}\right\rangle\right|^2 \\ &\quad\times\delta^{(3)}(\vec{p}_{^3\mathrm{He}} + \vec{p}_\pi) \\ &\quad\times\delta\left(M_{^3_\Lambda\mathrm{H}} - M_{^3\mathrm{He}} - \frac{\vec{p}^{\,2}_{^3\mathrm{He}}}{2M_{^3\mathrm{He}}} - E_\pi\right). \end{aligned} \tag{5}$$

The expression involves averaging over the initial, $m_{^3_\Lambda\mathrm{H}}$, and summation over the final, $m_{^3\mathrm{He}}$, spin projections of the (hyper)nuclear states Ψ and the integration over the two final ^{3}He and π^- momenta, $\vec{p}_{^3\mathrm{He}}$ and $\vec{p}_\pi$, is accompanied by the corresponding phase factor, with $E_\pi = \sqrt{m_\pi^2 + \vec{p}_\pi^{\,2}}$ the relativistic energy of the pion. The final π^--^{3}He scattering state $|\Psi_{^3\mathrm{He}}\phi_\pi\rangle$ is discussed in detail in Sec. II D. The isospin factor $\sqrt{3}$ in Eq. (5) accounts for the three final nucleons into which the Λ may transition and the Dirac delta functions ensure momentum and energy conservation by fixing the values of $\vec{p}_{^3\mathrm{He}}$ and the modulus of the outgoing pion momentum $\vec{p}_\pi$, where $M_{^3_\Lambda\mathrm{H}} = 2991$ MeV and $M_{^3\mathrm{He}} = 2809$ MeV in the argument are the ${}^3_\Lambda$H and ^{3}He masses. Since there is no preferred spatial direction, we choose the quantization z axis in the direction of $\vec{p}_\pi$ and integrate out the remaining angular dependence as $\int \mathrm{d}\hat{p}_\pi = 4\pi$. Eq. (5) then becomes

$$\Gamma^{^3\mathrm{He}} = \frac{3}{4\pi}\frac{M_{^3\mathrm{He}}\,q_\pi}{M_{^3\mathrm{He}} + E_\pi}\sum_{m_{^3_\Lambda\mathrm{H}}}\sum_{m_{^3\mathrm{He}}}\left|\left\langle\Psi_{^3\mathrm{He}}\phi_\pi\middle|\hat{O}\middle|\Psi_{^3_\Lambda\mathrm{H}}\right\rangle\right|^2, \tag{6}$$

where the pion momentum is kinematically fixed by

$$\begin{aligned} q_\pi &= \sqrt{2M_{^3\mathrm{He}}}\sqrt{M_{^3_\Lambda\mathrm{H}} - \sqrt{m_\pi^2 + 2M_{^3\mathrm{He}}M_{^3_\Lambda\mathrm{H}} - M_{^3\mathrm{He}}^2}} \\ &= 114.4\ \mathrm{MeV} \end{aligned} \tag{7}$$

for average pion mass $m_\pi = 138.04$ MeV and corresponds to pion energy $E_\pi = \sqrt{m_\pi^2 + q_\pi^2} = 179.3$ MeV.

C. Weak-decay operator

The transition operator in Eq. (6) originates from an effective Lagrangian density for the weak $\Lambda \to N\pi$ transitions

$$\mathcal{L}_{\Lambda N\pi} = G_F m_\pi^2\,\bar{\psi}_N(\mathcal{A}_\Lambda + \mathcal{B}_\Lambda\gamma_5)(\vec{\tau}\cdot\vec{\pi})\,\psi_\Lambda, \tag{8}$$

where $G_F m_\pi^2 = 2.21 \times 10^{-7}$; $\vec{\tau}$ are the isospin Pauli matrices; and ψ_Λ, ψ_N, and $\vec{\pi}$ are the Λ, nucleon, and isovector pion fields, respectively. The $\mathcal{A}_\Lambda = 1.024$ and $\mathcal{B}_\Lambda = -9.431$ are the parity-violating (PV) spin-dependent and parity-conserving (PC) spin-independent $\Lambda \to N\pi$ amplitudes. Values of these amplitudes were fixed by the lifetime of free Λ and the PC/PV decay rates ratio, $\Gamma_{\mathrm{PC}}/\Gamma_{\mathrm{PV}} = 0.203$, determined from the BESIII value of the $\Lambda \to p\pi^-$ asymmetry parameter [33]. The empirical $\Delta T = \frac{1}{2}$ rule, discussed in Sec. II A, is incorporated formally in Eq. (8) by adding $\vec{\tau}$ at the $\Lambda N\pi$ vertex, introducing a spurious $|\frac{1}{2}, -\frac{1}{2}\rangle$ isospin to the Λ hyperon, and assuming isospin conservation [21].

In its nonrelativistic form, the transition operator

$$\hat{O} = i\sqrt{2}G_F m_\pi^2\left(\mathcal{A}_\Lambda + \frac{\mathcal{B}_\Lambda}{2\overline{M}_{\Lambda N}}\vec{\sigma}\cdot\vec{q}_\pi\right)\hat{P}^{(\Lambda)}_{t_{12}=0}, \tag{9}$$

derived from the Lagrangian density (8), acts on the $A = 3$ wave functions and is responsible for the transition of the Λ hyperon in ${}^3_\Lambda$H to a proton in ^{3}He. The factor $\sqrt{2}$ is due to the spurious isospin of the Λ, and the projection operator $\hat{P}^{(\Lambda)}_{t_{12}=0}$ selects the isospin $t_{12} = 0, t_3 = 0$ ΛNN channels in the ${}^3_\Lambda$H wave functions. The $\vec{\sigma}$ are the Pauli matrices in spin space, $\vec{q}_\pi = q_\pi\hat{z}$ is the pion (on-shell) momentum, and $\overline{M}_{\Lambda N} = \frac{1}{2}(M_\Lambda + M_N)$, calculated using the average nucleon mass $M_N = 938.92$ MeV and $M_\Lambda = 1115.68$ MeV.

Considering the ΣNN admixtures in ${}^3_\Lambda$H induced by the $\Lambda N \leftrightarrow \Sigma N$ coupling in the hypernuclear Hamiltonian, new $\Sigma^- \to n\pi^-$ and $\Sigma^0 \to p\pi^-$ transitions become available and contribute to $\Gamma({}^3_\Lambda\mathrm{H} \to {}^3\mathrm{He} + \pi^-)$. To account for the $\Sigma \to N\pi$ contributions, we generalize the weak-decay operator as

$$\hat{O} \to \hat{O} + i\,G_F m_\pi^2\left(\frac{\sqrt{2}}{3}\mathcal{A}_{\Sigma^-} + \frac{1}{3}\mathcal{A}_{\Sigma^0}\right)\hat{P}^{(\Sigma)}_{t_{12}=1}. \tag{10}$$

The factors $\frac{\sqrt{2}}{3}$ and $\frac{1}{3}$ arise due to isospin Clebsh-Gordan (CG) coefficients when embedding the Σ^- and Σ^0 amplitudes within our $A = 3$ isospin states and $\hat{P}^{(\Sigma)}_{t_{12}=1}$ selects the isospin $t_{12} = 1, t_3 = 1$ ΣNN channels in the ${}^3_\Lambda$H wave functions. In Eq. (10), we neglect the PC part of $\Sigma \to N\pi$ amplitudes and fix the $\Sigma^- \to n\pi^-$ PV amplitude, $\mathcal{A}_{\Sigma^-} = 1.364$, to satisfy the Σ^- weak-decay lifetime value $\tau_{\Sigma^-} = 147.9$ ps [34]. In the case of Σ^0, the main decay mode is the electromagnetic $\Sigma^0 \to \Lambda\gamma$ transition, rendering the mesonic modes negligible. For the $\Sigma^0 \to p\pi^-$ amplitude we thus use the chiral-Lagrangian prediction to relate $\mathcal{A}_{\Sigma^0} = \frac{1}{\sqrt{2}}\mathcal{A}_{\Sigma^-}$ [34].

The explicit form of the transition operator (10) matrix elements between ${}^3_\Lambda$H and ^{3}He-π^- wave functions in Eq. (6) can be found in Appendix A.

D. Pion wave function

The distorted wave (DW) pion wave function $\phi_\pi(\vec{q}_\pi;\vec{r}) \equiv \langle \vec{r}\,|\phi_{\pi;\vec{q}_\pi}\rangle$ input to the transition matrix element in Eq. (5) was generated from a standard optical potential [35–37]. It evolves via FSI from a plane wave (PW) pion with momentum $\vec{q}$ in the ${}^3_\Lambda$H rest frame, and its argument $\vec{r} = \frac{2}{3}\vec{r}_3$ is identified with the coordinate of the third "active" baryon with respect to the center of mass (CM) of ^{3}He.

As a first approximation, the pion wave function is considered to be a PW with on-shell momentum $\vec{q}_\pi$ in the z direction, $\vec{q}_\pi = q_\pi\hat{z}$. Accordingly, a state $|q_\pi\hat{z}\rangle$ is inserted in the matrix element and fixes the momentum difference, $\vec{p}\,'_3 - \vec{p}_3$, between the two active baryons. The next step is to generate pion radial functions in the presence of a realistic pion-nucleus optical model. As in our previous publication [23], a natural starting point is provided by optical potentials that reproduce the vast amount of experimental strong interaction level shifts and widths in pionic atoms, essentially at zero energy.

Pion wave functions distorted by the pion-nucleus interaction are obtained by calculating pion-nucleus bound states in standard complex optical potentials. In our previous publication [23] we used global fits to pionic atoms derived from least-squares fits to 100 pionic atom data from Ne to U. In the present work we have extended the database by including eight additional species below Ne, including also ^{3}He. The new potential parameters [38] are consistent with those used in our previous publication and the added χ^2 for 16 points was 14.5. For ^{3}He we found $\chi^2 = 1.8$ for two points. Moving over to the true energy of the pion in the present process is relatively simple as described below.

The commonly accepted pion-nucleus optical potential is made of an s-wave term and a p-wave term, each containing a real part linear in the nuclear density and a complex part quadratic in density, representing pion absorption on two nucleons. The real coefficients turned out to be close to the corresponding spin- and isospin-dependent amplitudes for the free pion-nucleon interaction at threshold whereas the complex coefficients were phenomenological, with poorly determined real parts. Consequently we could set these real parts to zero without affecting the quality of fits to experiment. Then the real coefficients could be identified with the corresponding free pion-nucleon amplitudes at threshold. To extrapolate from near threshold to $q_\pi = 114.4$ MeV in the π^--^{3}He CM system we revised the above πN linear-density terms using energy-dependent scattering amplitudes from the SAID package [39]. For the nonlinear terms, we extrapolated their threshold values using as an additional point fits to $\pi^\pm$ elastic scattering at $T_{\rm Lab} = 21.5$ MeV on Si, Ca, Ni, and Zr [40,41]. This resulted in a practically vanishing value of the s-wave quadratic term and a 65% increase of the p-wave term.

Expanding $\phi_\pi(\vec{q}_\pi;\vec{r})$ in our calculations in partial waves l_π, and recalling the spin-parity $J^P = \frac{1}{2}^+$ of both ^{3}He and ${}^3_\Lambda$H, it follows that the only values allowed are $l_\pi = 0, 2$. Numerically we find a negligible $l_\pi = 2$ contribution of order 0.1%, proceeding exclusively through the relatively minor PC amplitude which in total contributes $\lesssim 3\%$ to $\Gamma({}^3_\Lambda\text{H} \to {}^3\text{He} + \pi^-)$.

To insert the DW, derived in position space, in the transition matrix element, we first Fourier transform it to momentum space using

$$\tilde{\phi}_{l_\pi}(k) = Y^*_{l_\pi 0}(\hat{z})\frac{2}{\pi\, q_\pi}\int_0^\infty \mathrm{d}r\, r\, j_{l_\pi}(kr)\phi_{l_\pi}(q_\pi;r) \tag{11}$$

and express the π^- state $|\phi_\pi\rangle$ in Eq. (5) in terms of partial-wave basis states $|k\, l_\pi\rangle$ as

$$|\phi_\pi\rangle = \sum_{l_\pi}\int \mathrm{d}k\, k^2\, \tilde{\phi}_{l_\pi}(k)|k\, l_\pi\rangle. \tag{12}$$

The state is normalized as

$$\sum_{l_\pi}\int \mathrm{d}k\, k^2\left|\tilde{\phi}_{l_\pi}(k)\right|^2 = 1. \tag{13}$$

All details of the derivation and numerical implementation are given in Appendix B.

E. Nuclear and hypernuclear wave functions

The initial- and final-state wave functions of ${}^3_\Lambda$H and ^{3}He in Eq. (5) were computed within the *ab initio* no-core shell model (NCSM) [42,43]. In this approach, nuclei and hypernuclei are described as systems of A nonrelativistic point-like particles interacting through realistic nucleon-nucleon (NN), three-nucleon (NNN), and hyperon-nucleon (YN) interactions. In NCSM, the many-body wave function is expanded in a complete set of harmonic oscillator (HO) basis states characterized by the HO frequency $\hbar\omega$ and truncated by the maximum number $N_{\rm max}$ of HO excitations above the lowest configuration allowed by Pauli principle,

$$|\Psi^{J^\pi T}\rangle = \sum_{N=0}^{N_{\rm max}}\sum_\lambda c^{J^\pi T}_{N\lambda}\,|N\lambda JT\rangle. \tag{14}$$

Here, N is the total number of HO excitations of all particles and $J^\pi T$ are the total angular momentum, parity, and isospin. The quantum number λ labels all additional quantum numbers and the sum over N is restricted by parity to an even or odd sequence. The energy eigenstates are obtained by solving the Schrödinger equation.

In this work we employed a version of NCSM formulated in translationally invariant relative Jacobi-coordinate HO basis, which is suitable for dealing with few-body systems. Different sets of Jacobi coordinates can be employed, one

of which is particularly convenient for the construction of HO basis states antisymmetric with respect to all nucleons and evaluation of the matrix element in (5). For $A = 3$ (hyper)nuclear systems, we introduce

$$\begin{aligned}\vec{p}_{\rm CM} &= \vec{p}_1 + \vec{p}_2 + \vec{p}_3,\\ \vec{p}_{12} &= \frac{1}{m_1+m_2}(m_2\,\vec{p}_1 - m_1\,\vec{p}_2),\\ \vec{p}_3 &= \frac{1}{\sum_{i=1}^{3} m_i}[m_3(\vec{p}_1+\vec{p}_2) - (m_1+m_2)\,\vec{p}_3],\end{aligned} \tag{15}$$

where m_i and $\vec{p}_i$ are the mass and momentum of particle $i = 1, 2, 3$. In (15), $\vec{p}_{\rm CM}$ is the CM momentum, $\vec{p}_{12}$ is the relative momentum of two nucleons, and $\vec{p}_3$ is the momentum of the third particle (nucleon or hyperon) with respect to the CM of the nucleon pair.

The use of relative coordinates allows us to separate out and omit the CM degrees of freedom. Consequently, the HO basis states in (14) for ${}^{3}_{\Lambda}$H can be constructed as

$$|N\lambda JT\rangle_{{}^{3}_{\Lambda}\rm H} = |(\lambda_{12},\lambda_3)JT\rangle, \tag{16}$$

where $|\lambda_{12}\rangle \equiv |n_{12}(l_{12}s_{12})j_{12}t_{12}\rangle$ are two-nucleon HO states, depending on the coordinate $\vec{p}_{12}$, with radial n_{12}, orbital l_{12}, spin s_{12}, angular momentum j_{12}, and isospin t_{12} quantum numbers. Antisymmetry of the NN states with respect to the nucleon interchange is achieved by imposing $(-1)^{l_{12}+s_{12}+t_{12}} = -1$. Similarly, the HO states $|\lambda_3\rangle \equiv |n_3(l_3s_3)j_3t_3\rangle$ depending on the coordinate $\vec{p}_3$ describe the relative motion of the hyperon (Λ or Σ for $t_3 = 0, 1$) with respect to the CM of the NN pair. The number of HO excitations in the state (16) is $N = 2\,n_{12} + l_{12} + 2\,n_3 + l_3$ and the parentheses denote angular momentum and isospin coupling. In the case of ^{3}He, the HO states in (14) have to be antisymmetric with respect to exchanges of all nucleons. The antisymmetrization procedure, when relative Jacobi coordinates are employed, is discussed in detail, e.g., in Ref. [44]. The fully antisymmetric HO states are obtained as linear combinations of HO states with a lower degree of antisymmetry,

$$|N\lambda JT\rangle_{{}^{3}\rm He} = \sum_{\tilde{\lambda}} C^{NJT}_{\lambda\tilde{\lambda}}\,|(\tilde{\lambda}_{12},\tilde{\lambda}_3)JT\rangle, \tag{17}$$

where the expansion coefficients $C^{NJT}_{\lambda\tilde{\lambda}}$ are the coefficients of fractional parentage. Here, analogously to Eq. (16), $|\tilde{\lambda}_{12}\rangle$ depending on $\vec{p}_{12}$ is an antisymmetric HO state describing the relative motion of the NN pair, and $|\tilde{\lambda}_3\rangle$ depending on $\vec{p}_3$ is associated with the relative motion of the third nucleon with respect to the CM of the NN pair.

To evaluate the matrix elements of the weak-decay operator between the initial and final states, we project the ${}^{3}_{\Lambda}$H and ^{3}He NCSM wave functions (14) onto a momentum-space partial-wave basis as

$$|\Psi^{J^\pi T}\rangle = \sum_{\alpha}\int {\rm d}p_{12}\,p_{12}^2\,{\rm d}p_3\,p_3^2\,\psi_\alpha(p_{12},p_3)|p_{12}\,p_3\,\alpha\rangle. \tag{18}$$

Here, $p_{12(3)} = |\vec{p}_{12(3)}|$, and α labels the JT-coupled three-particle channels,

$$|\alpha\rangle \equiv |((l_{12}s_{12})j_{12}(l_3s_3)j_3)JM\rangle|(t_{12}t_3)TM_T\rangle, \tag{19}$$

where M and M_T are the projections of the total angular momentum and isospin. The labeling of momenta and two- and one-particle spin, isospin, and angular momentum quantum numbers follows the same scheme as in the case of HO basis states in Eqs. (16) and (17). The coefficient functions ψ_α in Eq. (18) are combinations of the expansion coefficients in (14), (17), and momentum-space radial HO functions. They are normalized as

$$\sum_{\alpha}\int {\rm d}p_{12}\,p_{12}^2\,{\rm d}p_3\,p_3^2|\psi_\alpha(p_{12},p_3)|^2 = 1. \tag{20}$$

F. Input nuclear and hypernuclear interactions

In this work, we utilized realistic $NN+NNN$ and YN interactions derived from χEFT. We did not apply any renormalization, such as the similarity renormalization group or Lee-Suzuki transformation, to either of the interactions. In particular, we employed the NNLO$_{\rm sim}$ nuclear forces constructed at next-to-next-to-leading order (NNLO) [45] which were optimized to simultaneously reproduce NN as well as πN scattering data, the binding energies and charge radii of ^{2,3}H and ^{3}He, the quadrupole moment of ^{2}H, and the β-decay half-life of ^{3}H. NNLO$_{\rm sim}$ is a family of 42 different interactions where each potential is associated with one of seven regulator cutoffs, $\Lambda_{NN} = 450, 475, \ldots, 575, 600$ MeV, together with six different maximum scattering energies in the laboratory frame, $T_{\rm Lab}^{\rm max} = 125, 158, \ldots, 257, 290$ MeV, truncating the experimental NN cross sections used to constrain the respective interaction. We note that the 42 parametrizations of the nuclear force give equally good descriptions of the calibration data. Using all of them allows us to expose the magnitude of systematic nuclear-model uncertainties resulting from the incomplete knowledge of the nuclear interaction. In this work we are mainly interested in the wave function of ^{3}He and the "core nucleus" ^{2}H. Since certain low-energy properties of ^{2}H and ^{3}He were included in the pool of fit data, their energies are accurately described for all these interactions: $E_{{}^{2}{\rm H},{}^{3}{\rm He}} = -2.224^{(+0)}_{(-1)}, -7.717^{(+17)}_{(-21)}$ MeV [45]. For NNLO$_{\rm sim}$, the NCSM-calculated ground-state (g.s.) energies of ^{2}H and ^{3}He exhibit a weak dependence on the model-space truncation $N_{\rm max}$ and the HO frequency $\hbar\omega$, as shown in Fig. 2 for $NN+NNN$ interaction with $\Lambda_{NN} = 500$ MeV and $T_{\rm Lab}^{\rm max} = 290$ MeV. The g.s. energies are converged within few keV already at $N_{\rm max} \approx 30$ for a wide range of HO frequencies $\hbar\omega$.

For the YN interaction we employed the Bonn-Jülich coupled-channel flavor-SU(3)-based χEFT model [46]. This potential is constructed at leading order (LO) and regularized by a smooth momentum cutoff Λ_{YN} ranging from 550 to 700 MeV. Its parameters were determined from fits to the measured YN scattering cross sections, additionally constrained by allowing for a bound $J^\pi = \frac{1}{2}^+$ ${}^{3}_{\Lambda}$H state. This interaction was found to be consistent with the experimental value of the Λ separation energy in ${}^{3}_{\Lambda}$H, employing the NCSM [43] as well as Faddeev [47] approaches. NCSM calculations of ${}^{3}_{\Lambda}$H g.s.

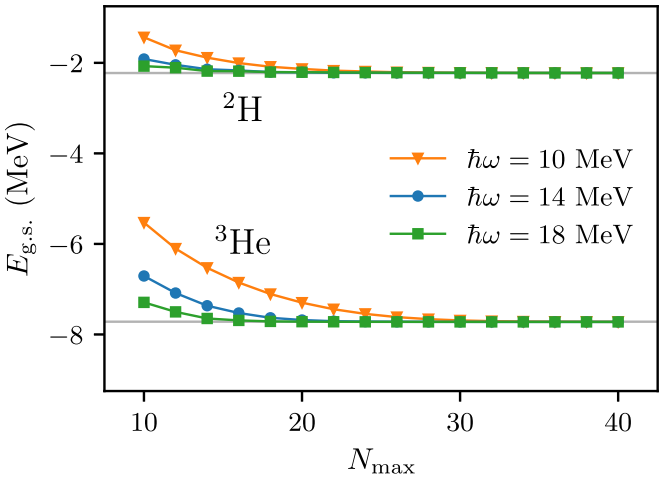

FIG. 2. Dependence of ^{2}H and ^{3}He g.s. energies $E_{\text{g.s.}}$ on the NCSM model-space truncation $10 \leqslant N_{\max} \leqslant 40$ for several values of the HO frequency, $\hbar\omega = 10$, 14, and 16 MeV, calculated using the NNLO$_{\text{sim}}$($\Lambda_{NN} = 500$ MeV, $T_{\text{Lab}}^{\max} = 290$ MeV) interaction. Indicated by the gray horizontal lines are the corresponding experimental values.

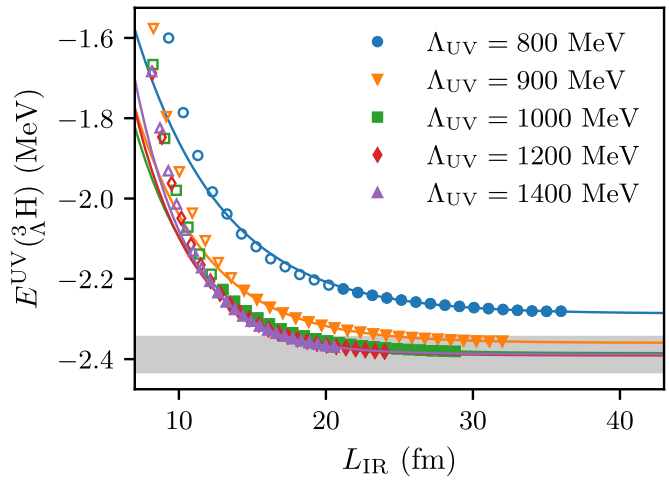

FIG. 3. NCSM $^3_\Lambda$H g.s. energies $E^{\text{UV}}(^3_\Lambda\text{H})$ (empty and filled symbols) as functions of the IR length L_{IR} (up to $N_{\max} = 68$) calculated using the NNLO$_{\text{sim}}$($\Lambda_{NN} = 500$ MeV, $T_{\text{Lab}}^{\max} = 290$ MeV) and LO YN ($\Lambda_{YN} = 600$ MeV) interactions for several fixed values of the UV cutoff Λ_{UV}, together with their extrapolations (solid lines). Only the points marked by filled symbols, corresponding to particle-stable $^3_\Lambda$H configurations, $E(^3_\Lambda\text{H}) < E(^2\text{H})$, are included in the fits. The world-average value of the measured $^3_\Lambda$H energy $E^{\text{exp.}}(^3_\Lambda\text{H}) = -2.389(43)$ MeV [6] is indicated by the gray band.

energy exhibit a stronger, undesired dependence on the model-space truncation $N_{\max}$ and the HO frequency $\hbar\omega$ [48,49]. The slow convergence can be attributed to the small Λ separation energy and, accordingly, the long tail of the $^3_\Lambda$H wave function in position space. The truncation of the HO basis in terms of $N_{\max}$ and $\hbar\omega$ can be translated into associated infrared (IR) and ultraviolet (UV) scales. For NCSM, the corresponding IR and UV scales, L_{IR} and Λ_{UV}, can be extracted by studying the kinetic energy spectrum and used to extrapolate results obtained in truncated model spaces to infinite model space ($L_{\text{IR}} \to \infty$) [49,50]. The LO correction for energies and the expected magnitude of subleading corrections σ_{IR} [51] are

$$E(L_{\text{IR}}) = E_\infty + a_0\, e^{-2k_\infty L_{\text{IR}}},$$
$$\sigma_{\text{IR}} \propto \frac{e^{-2k_\infty L_{\text{IR}}}}{k_\infty L_{\text{IR}}}. \tag{21}$$

The extrapolated energy E_∞, together with a_0 and k_∞, are parameters determined from fits to the NCSM-calculated energies with weights proportional to the inverse of σ_{IR}. Here we apply an iterative procedure with the weights fixed in each optimization until self-consistency for k_∞ in Eq. (21) is reached. Note that this prescription for IR extrapolation slightly differs and thus results in marginal discrepancies in comparison with the one previously employed by us in Ref. [23]. In addition, UV corrections to Eq. (21) can be significant and depend on details of the nuclear and YN interactions [52]. For interactions with nonlocal momentum regulators, like those used in this work, Λ_{UV} should significantly exceed Λ_{NN} and Λ_{YN}. A large-enough Λ_{UV} scale can be identified by performing calculations at a fixed Λ_{UV}—by choosing appropriate ($N_{\max}$, $\hbar\omega$) model-space parameters [51]—and monitoring the dependence of results, such as the extrapolated energy $E_\infty(\Lambda_{\text{UV}})$ in Eq. (21), on the selected Λ_{UV} scale. We find that $\Lambda_{\text{UV}} = 1200$ MeV is sufficient to achieve UV convergence; see also Ref. [49]. This is demonstrated in Fig. 3 where the $^3_\Lambda$H g.s. energy $E(^3_\Lambda\text{H})^{\text{UV}}$ is shown as a function of the IR length L_{IR} for several fixed values of the UV scale $800 \leqslant \Lambda_{\text{UV}} \leqslant 1400$ MeV (empty and filled symbols). The NCSM calculations were performed with model space truncation up to $N_{\max} = 68$ using the NNLO$_{\text{sim}}$($\Lambda_{NN} = 500$ MeV, $T_{\text{Lab}}^{\max} = 290$ MeV) and LO YN ($\Lambda_{YN} = 600$ MeV) interactions. The energy is clearly converging with increasing the size of the model space. The extrapolated values, E_∞^{UV}, exhibit a marginal dependence on the UV scale of the HO basis for $\Lambda_{\text{UV}} \gtrsim 1000$ MeV; see Table I in Sec. III A. In fact, for $E(^3_\Lambda\text{H})$ no extrapolation is necessary since the NCSM calculations performed at $N_{\max} \approx 68$ are converged with a precision of few keV. For example, by fixing $\Lambda_{\text{UV}} = 1000,\ 1200$ MeV, which implies $\hbar\omega = 7.299,\ 10.510$ MeV for $N_{\max} = 68$, we obtain $E^{1000,1200}(^3_\Lambda\text{H}) = -2.3807,\ -2.3814$ MeV, while the

TABLE I. Extrapolated $^3_\Lambda$H g.s. energies E_∞ and two-body π^- decay rates Γ_∞ for several values of the HO basis UV scale, calculated using the NNLO$_{\text{sim}}$($\Lambda_{NN} = 500$ MeV, $T_{\text{Lab}}^{\max} = 290$ MeV) and LO YN ($\Lambda_{YN} = 600$ MeV) interactions. The rates are evaluated using pion DW and considering the ΣNN contributions. The values of the (extrapolated) Λ separation energies, $B_\Lambda \equiv E(^2\text{H}) - E_\infty$, are obtained using converged deuteron g.s. energies $E(^2\text{H})$ at the corresponding Λ_{UV} scale.

Λ_{UV} (MeV)	800	900	1000	1200	1400
E_∞ (MeV)	−2.287	−2.359	−2.385	−2.391	−2.388
$E(^2\text{H})$ (MeV)	−2.221	−2.224	−2.224	−2.224	−2.224
B_Λ (MeV)	0.066	0.135	0.161	0.167	0.164
Γ_∞ (GHz)	0.944	1.180	1.253	1.276	1.289

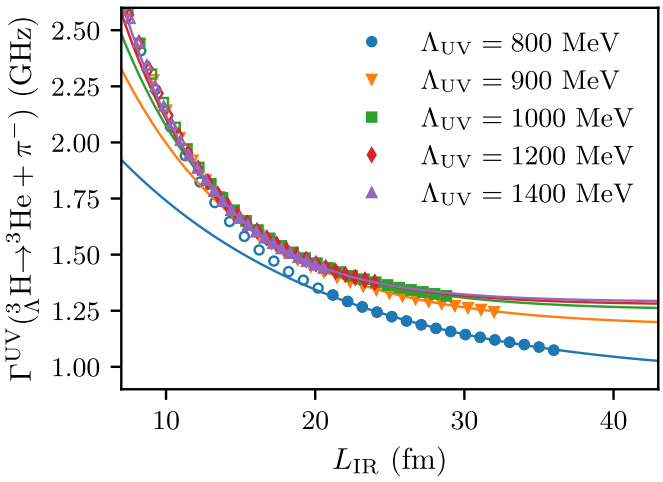

FIG. 4. NCSM $^3_\Lambda$H two-body π^- rates $\Gamma(^3_\Lambda{\rm H}\to{}^3{\rm He}+\pi^-)$ (empty and filled symbols) as functions of the IR length $L_{\rm IR}$ (up to $N_{\rm max}=68$) calculated using the NNLO$_{\rm sim}$($\Lambda_{NN}=500$ MeV, $T^{\rm max}_{\rm Lab}=290$ MeV) and LO YN ($\Lambda_{YN}=600$ MeV) interactions for several fixed values of the UV cutoff $\Lambda_{\rm UV}$, together with their extrapolations (solid lines). The rates are evaluated using pion DW and considering the ΣNN contributions. Only the points marked by filled symbols, corresponding to particle-stable $^3_\Lambda$H configurations, are included in the fits. The NCSM model-space parameters for ^{3}He are fixed at $N_{\rm max}=36$ and $\hbar\omega=14$ MeV, corresponding to a well-converged wave function.

extrapolated infinite-space result estimated using Eq. (21) is $E_\infty^{1000,1200}=-2.385,\ -2.391$ MeV. However, an adapted version of the IR-extrapolation scheme (21) will be applied in Sec. III A to the $^3_\Lambda$H two-body π^- decay rate in Eq. (5), which is found to have slightly different NCSM model-space convergence properties.

Most of the NCSM calculations in this work are performed for a particular (hyper)nuclear Hamiltonian with fixed values of $\Lambda_{NN}=500$ MeV, $T^{\rm max}_{\rm Lab}=290$ MeV, and $\Lambda_{YN}=600$ MeV cutoffs. A detailed analysis of theoretical uncertainties associated with these cutoffs for relevant observables is presented in Sec. III D.

III. RESULTS

A. Two-body π^- decay rate $\Gamma(^3_\Lambda{\rm H}\to{}^3{\rm He}+\pi^-)$

Employing the NCSM ^{3}He and $^3_\Lambda$H wave functions calculated using the NNLO$_{\rm sim}$($\Lambda_{NN}=500$ MeV, $T^{\rm max}_{\rm Lab}=290$ MeV) and LO YN ($\Lambda_{YN}=600$ MeV) interactions, we now proceed to calculate the two-body π^- decay rate $\Gamma(^3_\Lambda{\rm H}\to{}^3{\rm He}+\pi^-)$ in Eq. (5). While for ^{3}He the NCSM model-space parameters were fixed at $N_{\rm max}=36$ and $\hbar\omega=14$ MeV, corresponding to a well-converged wave function, for $^3_\Lambda$H we employ wave functions generated up to $N_{\rm max}=68$ and HO frequencies $\hbar\omega$ which correspond to several fixed UV cutoffs $\Lambda_{\rm UV}$, in order to examine the IR and UV convergence of $\Gamma(^3_\Lambda{\rm H}\to{}^3{\rm He}+\pi^-)$. The calculated two-body rates $\Gamma(^3_\Lambda{\rm H}\to{}^3{\rm He}+\pi^-)$ are shown in Fig. 4 as functions of the IR HO basis length scale $L_{\rm IR}$ for $\Lambda_{\rm UV}=800$, 900, 1000, 1200, and 1400 MeV. The rates include the effect of the distortion of the outgoing pion wave, as well as contributions of the $\Sigma\to N\pi$ transitions due to ΣNN admixtures in $^3_\Lambda$H. They exhibit an exponential decrease with $L_{\rm IR}$ similar to, although slower than, the $^3_\Lambda$H g.s. energies in Fig. 3. The solid lines in Fig. 4 correspond to the IR extrapolations into infinite NCSM model space. The extrapolations were performed using an adapted version of Eq. (21) and included only the points marked by filled symbols, corresponding to particle-stable $^3_\Lambda$H configurations. The extrapolated ($L_{\rm IR}\to\infty$) two-body π^- rates Γ_∞, as well as the $^3_\Lambda$H g.s. energies E_∞, are listed in Table I. Both the extrapolated energies and rates exhibit a rather small dependence on the UV cutoff for $1000\lesssim\Lambda_{\rm UV}\lesssim1200$ MeV. Also listed in Table I are the (extrapolated) Λ separation energies in $^3_\Lambda$H calculated using E_∞ and IR converged ^{2}H g.s. energies $E(^2{\rm H})$ at the corresponding cutoff values $\Lambda_{\rm UV}$. As demonstrated in Fig. 4 and Table I, working at a fixed value of $\Lambda_{\rm UV}=1200$ MeV provides a good compromise between minimization of the UV corrections and reliable IR extrapolation. The small increase in E_∞ for $\Lambda_{\rm UV}=1400$ MeV indicates that higher-order IR corrections to Eq. (21) become relevant for $\Lambda_{\rm UV}\gtrsim1400$ MeV.

B. Main contributions to $\Gamma(^3_\Lambda{\rm H}\to{}^3{\rm He}+\pi^-)$

Out of all three-body channels α in Eq. (19), only few contribute significantly to the wave functions of ^{3}He and $^3_\Lambda$H. The dominant component of the hypertriton wave function is a deuteronlike core with $l_{12}=t_{12}=0$, $s_{12}=j_{12}=1$ coupled to a Λ hyperon ($t_3=0$) s-wave state. It contributes by $\approx96\%$ to the square of the norm of the $^3_\Lambda$H wave function. The analogous channel in ^{3}He accounts for $\approx47\%$, with additional $\approx47\%$ originating from the $l_{12}=s_{12}=l_3=0$ component with isospin $t_{12}=1$. Consequently, the largest contribution to the decay rate $\Gamma(^3_\Lambda{\rm H}\to{}^3{\rm He}+\pi^-)$ is generated by the $^{(2t_{12}+1)(2s_{12}+1)}l_{12\,j_{12}}={}^{13}S_1$, $l_3=0$ components in the wave functions. By constraining the decay rate to only these two components, $\psi_{^{13}S_1,l_3=t_3=0}(^3_\Lambda{\rm H})$ and $\psi'_{^{13}S_1,l_3=0}(^3{\rm He})$, and considering π^- PW, Eq. (6) reduces to a simpler expression,

$$\Gamma^{^3{\rm He}}_{^{13}S_1}=\frac{3}{4\pi}\frac{\left(G_F m_\pi^2\right)^2 M_{^3{\rm He}}\,q_\pi}{M_{^3{\rm He}}+E_\pi}\left(\mathcal{A}_\Lambda^2+\frac{1}{36}\frac{\mathcal{B}_\Lambda^2\,q_\pi^2}{\overline{M}_{\Lambda N}^2}\right)\times\left|\int{\rm d}p'_{12}\,p'^2_{12}\int{\rm d}p'_3\,p'^2_3\int{\rm d}\cos\theta_{p'_3}\times\psi_{^{13}S_1,l_3=t_3=0}\left(p'_{12},\left|p'_3\hat{p}'_3+\frac{2}{3}\vec{q}_\pi\right|\right)\times\psi'_{^{13}S_1,l_3=0}(p'_{12},p'_3)\right|^2. \tag{22}$$

For $\Lambda_{\rm UV}=1200$ MeV, Eq. (22) yields $\Gamma^{^3{\rm He}}_{^{13}S_1}=1.152$ GHz after extrapolation, as listed in Table II. This PW value differs merely by $\approx4\%$ from 1.108 GHz in the full calculation, partly due to cancellations discussed below.

Subleading contributions to $\Gamma(^3_\Lambda{\rm H}\to{}^3{\rm He}+\pi^-)$ for both π^- PW and DW are summarized in Table II. The remaining channel transitions due to $\Lambda\to p\pi^-$ increase the rate only by $\approx8\%$, to $\Gamma^{^3{\rm He}}=1.243$ GHz in PW. This increase originates mainly from the $^{13}D_1$, $l_3=0$ components of the wave

TABLE II. Extrapolated partial decay rates $\Gamma^{\rm UV}_{\infty}({}^{3}_{\Lambda}{\rm H} \to {}^{3}{\rm He}+\pi^-)$ (in GHz) at $\Lambda_{\rm UV}=1200$ MeV calculated using only the dominant ^{3}He and $^3_\Lambda$H wave function components (first row) and considering only the ΛNN channels in $^3_\Lambda$H (second row). Total rates including also the ΣNN components in $^3_\Lambda$H are in the last row. Probabilities are listed in percents and the rates in the third and fourth columns correspond to π^- PW and DW, respectively.

Channel restrictions	$P(^3{\rm He})$	$P(^3_\Lambda{\rm H})$	$\Gamma^{\rm UV}_{\rm PW}$	$\Gamma^{\rm UV}_{\rm DW}$
as in Eq. (22)	46.81	95.83	1.152	
$t_3(^3_\Lambda{\rm H})=0$	100.00	99.59	1.243	1.426
none	100.00	100.00	1.108	1.276

functions. In contrast, including also the ΣNN components in the $^3_\Lambda$H wave function and allowing for the $\Sigma^- \to n\pi^-$ and $\Sigma^0 \to p\pi^-$ transitions reduces the decay rate by ≈11% from 1.243 to 1.108 GHz, thus overcanceling the ≈8% increase from 1.152 to 1.243 GHz owing to the non-$^{13}S_1$ Λ amplitudes. Furthermore, replacing the outgoing π^--^{3}He PW by realistic π^--^{3}He DW increases each of the listed PW rates by ≈15%. However, despite providing substantial individual contributions, the combined effect of accounting for the two new mechanisms considered in this work, namely (i) including ΣNN components of $^3_\Lambda$H and (ii) introducing π^--^{3}He DW, is that they largely cancel each other with barely 3% net increase of $\Gamma(^3_\Lambda{\rm H} \to {}^3{\rm He}+\pi^-)$ from 1.243 to 1.276 GHz.

The ≈11% contribution to $\Gamma(^3_\Lambda{\rm H} \to {}^3{\rm He}+\pi^-)$ induced by a tiny ≈0.4% probability ΣNN component of $^3_\Lambda$H is a bit unexpected, particularly when compared to the ≈8% comparable contribution of the considerably stronger $^{13}D_1$ tensor component of order 3% probability in the initial $^3_\Lambda$H hypernucleus. However, recall that whereas the $^{13}D_1$ NN component in the final ^{3}He that supports the $\Lambda \to N\pi$ transition is of the same order as in $^3_\Lambda$H, the $^{31}S_0$ NN component in ^{3}He that supports the $\Sigma \to N\pi$ transition is almost of 50% probability. More importantly, since the two PV Λ and Σ weak decay amplitudes of Eq. (10) interfere upon forming their summed absolute value squared, even as small a ΣNN admixture probability as 0.4% in $^3_\Lambda$H may affect considerably the calculated $\Gamma(^3_\Lambda{\rm H} \to {}^3{\rm He}+\pi^-)$, which was found here to be reduced by ≈11% from that evaluated disregarding the ΣNN admixture. This effect is further assisted by the overlap of the relevant ΣNN $^3_\Lambda$H and ^{3}He wave-function components. Shown in Fig. 5 are the probability densities $\mathrm{p}_\alpha(p_3) \equiv \int {\rm d}p_{12}\, p_{12}^2\, p_3^2\, |\psi_\alpha(p_{12},p_3)|^2$ of the active baryon (N or Σ) relative momentum p_3 for the $\alpha = {}^{31}S_0, l_3{=}0$ ^{3}He and the dominant ΣNN $\alpha = {}^{31}S_0, l_3{=}0, t_3{=}1$ $^3_\Lambda$H wave-function components, together with the associated NN relative momentum p_{12} distributions $\mathrm{p}_\alpha(p_{12}) \equiv \int {\rm d}p_3\, p_3^2\, p_{12}^2\, |\psi_\alpha(p_{12},p_3)|^2$. The Σ momentum distribution in $^3_\Lambda$H is localized around a higher value of p_3, closer to the peak of the active-nucleon momentum distribution in ^{3}He compared to the $^{13}S_1, l_3=0$ Λ and N momentum distributions shown in Fig. 6.

C. Dependence of $\Gamma(^3_\Lambda{\rm H} \to {}^3{\rm He}+\pi^-)$ on B_Λ

While the UV convergence of extrapolated separation energies $E_\infty(^3_\Lambda{\rm H})$ and two-body decay rates

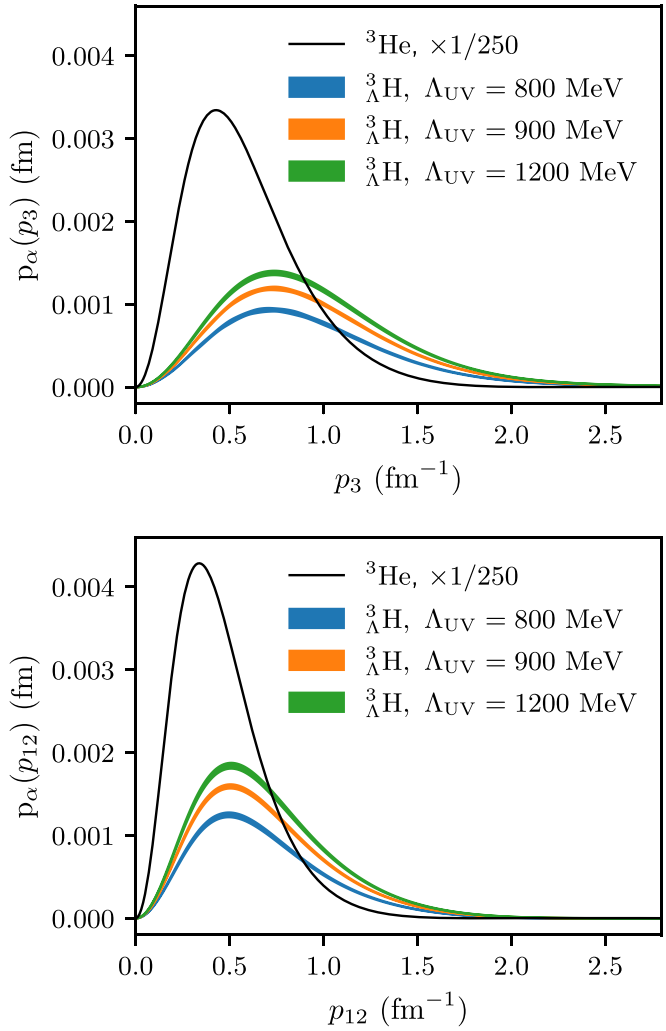

FIG. 5. Probability densities $\mathrm{p}_\alpha(p_3) \equiv \int {\rm d}p_{12}\, p_{12}^2\, p_3^2\, |\psi_\alpha(p_{12},p_3)|^2$ of the active baryon (N or Σ) relative momentum p_3 for the $\alpha = {}^{31}S_0, l_3{=}0$ ^{3}He and the dominant ΣNN $\alpha = {}^{31}S_0, l_3{=}0, t_3{=}1$ $^3_\Lambda$H wave-function components (top panel), together with the corresponding distributions $\mathrm{p}_\alpha(p_{12}) \equiv \int {\rm d}p_3\, p_3^2 p_{12}^2\, |\psi_\alpha(p_{12},p_3)|^2$ of the NN relative momentum p_{12} (bottom panel). The densities are calculated using the NNLO$_{\rm sim}$($\Lambda_{NN}=500$ MeV, $T^{\rm max}_{\rm Lab}=290$ MeV) and LO YN ($\Lambda_{YN}=600$ MeV) interactions. For $^3_\Lambda$H, each band corresponds to a particular value of the $\Lambda_{\rm UV}$ cutoff, while its width shows the variation with the model-space truncation $N_{\rm max}$ for $60 \leqslant N_{\rm max} \leqslant 68$. For ^{3}He, the NCSM model-space parameters are fixed at $N_{\rm max}=36$ and $\hbar\omega=14$ MeV, corresponding to a well-converged wave function. The $\mathrm{p}_\alpha(p_{12})$ and $\mathrm{p}_\alpha(p_3)$ distributions in ^{3}He are scaled by a factor of 1/250.

$\Gamma_\infty(^3_\Lambda{\rm H} \to {}^3{\rm He}+\pi^-)$ for $\Lambda_{\rm UV} \lesssim 1200$ MeV was not fully achieved (see Table I), it is evident from their $L_{\rm IR}$ dependence, shown in Figs. 2 and 3, that the calculations still give meaningful, sufficiently IR-converged results. The missing UV corrections to Eq. (21) depend only on short-range details of the employed interactions which are truncated by the $\Lambda_{\rm UV}$ cutoff. Nevertheless, the correlation between E_∞ and Γ_∞ appear to be robust, and their dependence on $\Lambda_{\rm UV}$ can thus be exploited to study the relationship of B_Λ and

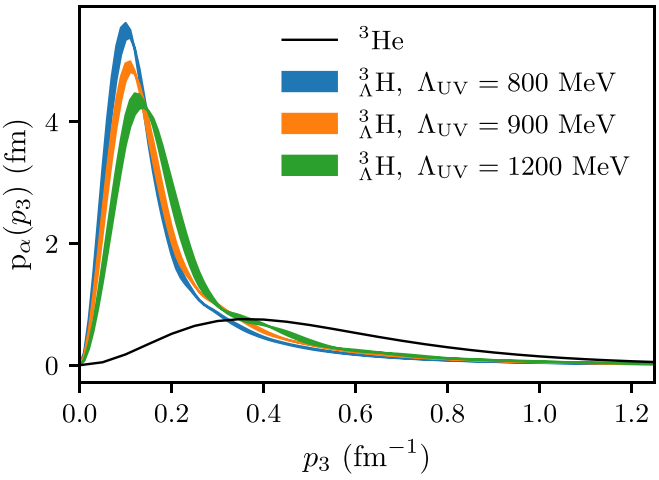

FIG. 6. Probability densities $\mathrm{p}_\alpha(p_3)$ as in Fig. 5 of the dominant $\alpha = {}^{13}S_1, l_3 = 0$ ^{3}He and $\alpha = {}^{13}S_1, l_3 = t_3 = 0$ $^3_\Lambda$H wave-function components as functions of the active baryon (N or Λ) relative momentum p_3. Note that $\int \mathrm{d}p_3\, \mathrm{p}_\alpha(p_3) \approx 47\%$ and 96% for ^{3}He and $^3_\Lambda$H, respectively.

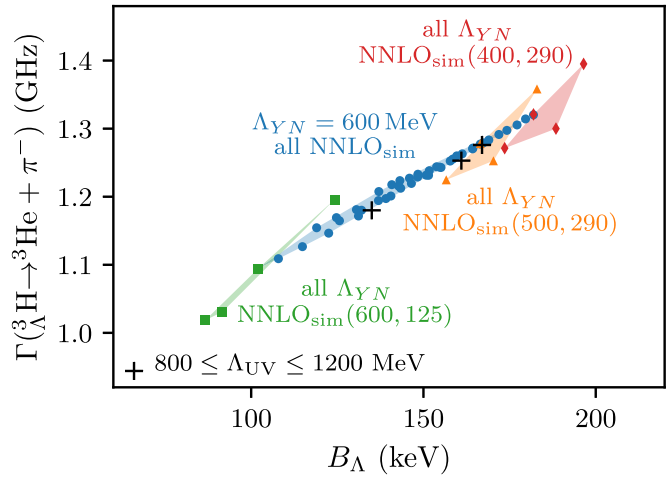

FIG. 7. Variation of the extrapolated Λ separation energies in $^3_\Lambda$H and decay rates $\Gamma(^3_\Lambda\mathrm{H} \to {}^3\mathrm{He} + \pi^-)$ with the Λ_{NN}, $T^{\rm max}_{\rm Lab}$ and Λ_{YN} cutoffs applied in the nuclear NNLO$_{\rm sim}$ and LO YN hypernuclear interactions. The rates are calculated including contributions from π^- DW and ΣNN contributions for $\Lambda_{\rm UV} = 1200$ MeV. The energies and rates are computed for a fixed value of $\Lambda_{YN} = 600$ MeV and all 42 NNLO$_{\rm sim}$ Hamiltonians (circles); and all cutoffs $\Lambda_{YN} = 550, 600, 650, 700$ MeV for fixed values of $(\Lambda_{NN}, T^{\rm max}_{\rm Lab}) = (600, 125)$ MeV (squares), (500, 290) MeV (triangles), and (400, 290) MeV (diamonds). Results obtained for different values of the HO basis UV scale $800 \leqslant \Lambda_{\rm UV} \leqslant 1200$ MeV with $(\Lambda_{NN}, T^{\rm max}_{\rm Lab}, \Lambda_{YN}) = (500, 290, 600)$ MeV are marked by black crosses. See text for details.

its associated $\Gamma(^3_\Lambda\mathrm{H} \to {}^3\mathrm{He} + \pi^-)$. In particular values of $800 \lesssim \Lambda_{\rm UV} \lesssim 1000$ MeV provide meaningfullyconverged rates calculated using well-converged $^3_\Lambda$H wave functions at lower values of B_Λ. Indeed, it will be shown in the following section that the relationship between the separation energy and the two-body rate at a particular value of $\Lambda_{\rm UV}$ is consistent with the one obtained by varying the parameters of the underlying nuclear and hypernuclear interactions.

The robust correlation between B_Λ and $\Gamma(^3_\Lambda\mathrm{H} \to {}^3\mathrm{He} + \pi^-)$ can be understood by means of the approximate expression for the two-body decay rate in Eq. (22). In particular, it can be traced back to the overlap between the $\psi_{^{31}S_0, l_3 = t_3 = 0}(p'_{12}, |p'_3 \hat{p}'_3 + \frac{2}{3}\vec{q}_\pi|)$ $^3_\Lambda$H and $\psi'_{^{31}S_0, l_3 = 0}(p'_{12}, p'_3)$ ^{3}He wave-function components. The $^3_\Lambda$H squared amplitude (probability distribution), $\mathrm{p}_\alpha(p_{12})$ (see Sec. III B), with $\alpha = {}^{13}S_1, l_3 = t_3 = 0$, is almost independent of $\Lambda_{\rm UV}$ and peaked at $p_{12} \approx 0.25$ fm^{-1}, very close to the peak in the corresponding amplitude of the $^{13}S_1$ component of the deuteron wave function. On the other hand, the analogous $^3_\Lambda$H squared amplitude $\mathrm{p}_\alpha(p_3)$ as a function of the relative momentum of the loosely bound Λ peaks at $p_3 \approx 0.1$ fm^{-1}, a value much lower than the corresponding momentum p'_3 of the active nucleon in ^{3}He. As larger $\Lambda_{\rm UV}$ cutoffs are considered, $\mathrm{p}_\alpha(p_3)$ peaks at larger momenta p_3, the Λ hyperon becomes more bound, and the overlap integral in Eq. (22) becomes larger. The density distributions $\mathrm{p}_\alpha(p_3)$ of the dominant components α of the ^{3}He and $^3_\Lambda$H wave functions are shown in Fig. 6 for $\Lambda_{\rm UV} = 800$, 1000, and 1200 MeV.

D. Theoretical (hyper)nuclear-structure uncertainties in $\Gamma(^3_\Lambda\mathrm{H} \to {}^3\mathrm{He} + \pi^-)$

The nuclear and hypernuclear wave functions entering the two-body π^- decay rate $\Gamma(^3_\Lambda\mathrm{H} \to {}^3\mathrm{He} + \pi^-)$ are associated with systematic uncertainties resulting from the selection of calibration data, the truncation of the chiral expansion, and possible regulator artifacts of the employed $NN + NNN$ and YN interaction models.

In order to estimate the limits of theoretical precision of relevant hypernuclear observables resulting from the nuclear model uncertainty, we employ the whole NNLO$_{\rm sim}$ family of 42 nuclear potentials; see Sec. II F. In addition, we also quantify variation of the observables related to the momentum regulator cutoff dependence of the LO YN potential. In particular, we focus on the spread of the predicted Λ separation energies B_Λ in $^3_\Lambda$H and the two-body $^3_\Lambda$H decay rates $\Gamma(^3_\Lambda\mathrm{H} \to {}^3\mathrm{He} + \pi^-)$. Results of this analysis are summarized in Fig. 7 where the extrapolated values of B_Λ and $\Gamma(^3_\Lambda\mathrm{H} \to {}^3\mathrm{He} + \pi^-)$ are obtained from NCSM calculations at $\Lambda_{\rm UV} = 1200$ MeV for $N_{\rm max}$ up to 68. The rates are computed including the contributions from π^- DW and $\Sigma \to N\pi$ modes. Results for a fixed value of the YN interaction regulator cutoff momentum $\Lambda_{YN} = 600$ MeV and all 42 NNLO$_{\rm sim}$ $NN + NNN$ potentials are presented by blue filled circles. The predicted Λ separation energy varies strongly, $100 \lesssim B_\Lambda \lesssim 180$ keV, and decreases with increasing the regulator cutoff Λ_{NN} and increases with increasing $T^{\rm max}_{\rm Lab}$ [48,49]. The two-body π^- rate is strongly correlated with B_Λ and varies in the range $1.1 \lesssim \Gamma(^3_\Lambda\mathrm{H} \to {}^3\mathrm{He} + \pi^-) \lesssim 1.3$ GHz. Surprisingly, this correlation is perfectly in line with the results obtained for different values of the HO basis UV scale listed in Table I and included in Fig. 7 for $800 \leqslant \Lambda_{\rm UV} \leqslant 1200$ MeV (black crosses). Also shown in Fig. 7 is the variation of B_Λ and $\Gamma(^3_\Lambda\mathrm{H} \to {}^3\mathrm{He} + \pi^-)$ with the YN regulator cutoff momentum Λ_{YN}.

We selected only 3 $\mathrm{NNLO_{sim}}$ Hamiltonians, two of which give the lowest and highest separation energies and rates, together with $\mathrm{NNLO_{sim}}(\Lambda_{NN} = 500\ \mathrm{MeV}, T_{\mathrm{Lab}}^{\mathrm{max}} = 290\ \mathrm{MeV})$. The energies and rates are calculated for $\Lambda_{YN} = 550$, 600, 650, and 700 MeV and fixed values of $(\Lambda_{NN}, T_{\mathrm{Lab}}^{\mathrm{max}}) =$ 600, 125 MeV (squares), (500, 290) MeV (triangles), and (400, 290) MeV (diamonds). In each group, the largest separation energy always occurs for $\Lambda_{YN} = 550$ MeV, decreases monotonically with Λ_{YN} for $550 \leqslant \Lambda_{YN} \leqslant 650$ MeV, and increases for $650 \leqslant \Lambda_{YN} \leqslant 700$ MeV. Note that the resulting combined spread of binding energies for all considered $(\Lambda_{NN}, T_{\mathrm{Lab}}^{\mathrm{max}}, \Lambda_{YN})$ cutoff combinations $\Delta B_\Lambda \approx 100$ keV is essentially of the same order as the experimental uncertainty, while $\Delta\Gamma(^3_\Lambda\mathrm{H} \to {}^3\mathrm{He} + \pi^-) \approx 0.4$ GHz.

Very recently, a comparable, although smaller, variation of B_Λ in $^3_\Lambda$H with the Λ_{NN} regulator cutoff momentum using higher-order χEFT NN interactions and LO YN ($\Lambda_{YN} =$ 600 MeV) was reported in [2]. In addition, the sensitivity of B_Λ to the employed nuclear interactions was also found there to decrease considerably when higher-order YN potentials were employed.

E. Hypertriton lifetime

To evaluate the total $^3_\Lambda$H decay rate and lifetime we employ the strategy described in detail in Sec. II A. Using the IR-extrapolated two-body π^- decay rate $\Gamma_\infty^{1200} =$ 1.276 GHz, associated with $B_\Lambda^{1200} = 167$ keV, we evaluate the inclusive π^- $^3_\Lambda$H decay rate $\Gamma_{\pi^-}(^3_\Lambda\mathrm{H})$ by means of the measured world-average BC branching ratio $R_3 = \Gamma(^3_\Lambda\mathrm{H} \to {}^3\mathrm{He} + \pi^-)/\Gamma_{\pi^-}(^3_\Lambda\mathrm{H}) = 0.35(4)$ [17]. By multiplying $\Gamma_{\pi^-}(^3_\Lambda\mathrm{H})$ by the $\Delta T = \frac{1}{2}$ factor of $\frac{3}{2}$ to include the neutral pion $^3_\Lambda$H decay channels, $\Gamma_\pi(^3_\Lambda\mathrm{H}) = \frac{3}{2}\,\Gamma_\pi^-(^3_\Lambda\mathrm{H})$, we derive the hypertriton lifetime corresponding to all pionic decay modes as $\tau_\pi(^3_\Lambda\mathrm{H}) = 1/\Gamma_\pi(^3_\Lambda\mathrm{H}) = 183(21)$ ps. Here and in what follows, the quoted lifetime uncertainty is purely statistical, arising from that of R_3. The nonmesonic $\Lambda N \to NN$ and pion true-absorption $\pi + NN \to NN$ contributions to the rate of 1.5% and 0.8%, respectively, further shorten the $^3_\Lambda$H lifetime. Accounting for their 2.3% combined increase of the rate, we obtain $\tau(^3_\Lambda\mathrm{H}) = 179(20)$ ps. This value is considerably shorter, by ≈32(8) percent, than the Λ lifetime in free space, $\tau_\Lambda = 263(2)$ ps. However, significantly longer $^3_\Lambda$H lifetime values, listed in Table III, are obtained by repeating the same procedure for the two-body π^- decay rates from Table I calculated at lower values of HO basis UV scale, $\Lambda_{\mathrm{UV}} = 800$, 900, and 1000 MeV. As argued in Secs. III C and III D, these rates are associated with smaller values of Λ separation energies B_Λ. It should be pointed out that for each of the derived $\tau(^3_\Lambda\mathrm{H})$ listed in Table III we have tacitly assumed the same value of branching ratio R_3, taken from experiment [17]. Note that we obtain for the least-bound $^3_\Lambda$H case at $\Lambda_{\mathrm{UV}} = 800$ MeV, a $\tau(^3_\Lambda\mathrm{H})$ value which is shorter than τ_Λ only by less than ≈10%.

Remarkably, this value, $\tau^{800}(^3_\Lambda\mathrm{H}) = 242(28)$ ps, is consistent with the most recent ALICE Collaboration's [8] reported lifetime $\tau^{\mathrm{ALICE}}(^3_\Lambda\mathrm{H}) = 253(11)(6)$ ps while its corresponding Λ separation energy $B_\Lambda^{800} = 66$ keV falls comfortably within the ALICE reported separation energy interval $B_\Lambda^{\mathrm{ALICE}} = 102(63)(67)$ keV. Within its R_3-induced uncertainty, $\tau^{800}(^3_\Lambda\mathrm{H})$ is also consistent with lifetime value derived in a fully three-body calculation in Ref. [21]. Similarly, the lifetime for $\Lambda_{\mathrm{UV}} = 1000$ MeV listed in Table III agrees well within measurement uncertainties with the HypHI Collaboration's lifetime value $\tau^{\mathrm{HypHI}}(^3_\Lambda\mathrm{H}) = 183^{+42}_{-32}(37)$ ps. In order to compare with STAR Collaboration's reported lifetime $142^{+24}_{-21}(29)$ ps [9] and their own value of Λ separation energy $B_\Lambda = 0.41(12)(12)$ MeV [53], we expand $\Gamma(^3_\Lambda\mathrm{H} \to {}^3\mathrm{He} + \pi^-)$ in powers of $\sqrt{B_\Lambda}$ as $a\sqrt{B_\Lambda} + b\,B_\Lambda$ and fix the two expansion coefficients by fitting to the B_Λ^{UV} and $\Gamma_\infty^{\mathrm{UV}}$ from Table I for $800 \leqslant \Lambda_{\mathrm{UV}} \leqslant 1200$ MeV. When extrapolated to $B_\Lambda = 410$ keV, we obtain $\tau(^3_\Lambda\mathrm{H}) = 158(18)$ ps. Had we considered STAR Collaboration's own value of $R_3^{\mathrm{STAR}} =$ 0.32(5)(8) [9], the estimated central value of $\tau(^3_\Lambda\mathrm{H}) =$ 145(51) GHz is almost coincident with STAR Collaboration's $\tau(^3_\Lambda\mathrm{H})$ central value. Moreover, the most recent STAR Collaboration's reported lifetime 221(15)(19) ps [11] is consistent with lower Λ separation energies $B_\Lambda \approx 90$ keV using $R_3 =$ 0.35(4), which are also plausible given the large measurement uncertainty in B_Λ.

Altogether, given the strong dependence of $\tau(^3_\Lambda\mathrm{H})$ on B_Λ and considering the large experimental uncertainty in B_Λ, none of the recent RHI reported $\tau(^3_\Lambda\mathrm{H})$ values can be excluded, but rather can be associated with its own underlying value of B_Λ.

TABLE III. Extrapolated Λ separation energies in $^3_\Lambda$H and associated lifetimes $\tau(^3_\Lambda\mathrm{H})$ (both in ps and τ_Λ, with their R_3-induced uncertainties) calculated using the $\mathrm{NNLO_{sim}}(\Lambda_{NN} = 500$ MeV, $T_{\mathrm{Lab}}^{\mathrm{max}} = 290$ MeV) and LO YN ($\Lambda_{YN} = 600$ MeV) interactions for several values of the HO basis UV scale, and extrapolated to the STAR Collaboration [53] reported value of B_Λ. The lifetimes are evaluated using $R_3 = 0.35(4)$ [17], the $\Delta T = \frac{1}{2}$ rule, and include a 2.3% correction from nonmesonic decay rate.

Λ_{UV} (MeV)	800	900	1000	1200	
B_Λ (keV)	66	135	161	167	410
$\tau(^3_\Lambda\mathrm{H})$ (ps)	242(28)	193(22)	182(21)	179(20)	158(18)
$\tau(^3_\Lambda\mathrm{H})$ (τ_Λ)	0.92(10)	0.73(8)	0.69(8)	0.68(8)	0.60(7)

IV. CONCLUSIONS

We performed a new microscopic calculation of the hypertriton π^- two-body decay rate $\Gamma(^3_\Lambda\mathrm{H} \to {}^3\mathrm{He} + \pi^-)$ employing $^3_\Lambda$H and ^{3}He three-body wave functions generated by the *ab initio* NCSM approach using realistic chiral YN and $NN + NNN$ interactions as the only input. Employing the $\Delta T = \frac{1}{2}$ rule and the experimental value of branching ratio $R_3 = \Gamma(^3_\Lambda\mathrm{H} \to {}^3\mathrm{He} + \pi^-)/\Gamma_{\pi^-}(^3_\Lambda\mathrm{H})$ to include the remaining π^0 and three- plus four-body $^3_\Lambda$H decay channels, we were able to deduce the $^3_\Lambda$H lifetime $\tau(^3_\Lambda\mathrm{H})$.

The following are the main findings and conclusions of this study:

(1) *Pionic FSI.* Considering the distortion of the emitted pion wave due to its strong-interaction attractive final-state interaction with the ^{3}He nucleus increases $\Gamma(^3_\Lambda\mathrm{H} \to {}^3\mathrm{He} + \pi^-)$ by ≈15%. A somewhat stronger

enhancement of ≈18% was found very recently in a pionless EFT calculation [30].

(2) *Effect of ΣNN admixtures.* Despite the negligible ΣNN-component admixture ($\lesssim 0.5\%$) in the ${}^3_\Lambda$H wave function, the $\Sigma \to N\pi$ transitions reduce $\Gamma({}^3_\Lambda\mathrm{H} \to {}^3\mathrm{He} + \pi^-)$ by ≈11% due to interference effects. It would be interesting to evaluate this effect using other χEFT YN potential versions than the LO version used here, thus adding the measured value of $\tau({}^3_\Lambda\mathrm{H})$ as a useful constraint on such YN potentials.

(3) *Relationship of B_Λ and $\Gamma({}^3_\Lambda\mathrm{H} \to {}^3\mathrm{He} + \pi^-)$.* The two-body π^- decay rate is found to be very sensitive to the Λ separation energy B_Λ in ${}^3_\Lambda$H, the value of which is rather poorly known experimentally and also suffers from large theoretical uncertainties.

(4) *Hypertriton lifetime.* Using the $\mathrm{NNLO_{sim}}(\Lambda_{NN} = 500$ MeV, $T_{\mathrm{Lab}}^{\max} = 290$ MeV) and LO YN ($\Lambda_{YN} = 600$ MeV) nuclear and hypernuclear interactions which yield $B_\Lambda^{\mathrm{th}}({}^3_\Lambda\mathrm{H}) = 167$ keV—consistent with the the world-average measured $B_\Lambda^{\mathrm{exp.}}({}^3_\Lambda\mathrm{H}) = 164(43)$ keV [6]—to calculate $\Gamma({}^3_\Lambda\mathrm{H} \to {}^3\mathrm{He} + \pi^-)$ and employing the branching ratio $R_3 = 0.35(4)$ [17], together with the empirical $\Delta T = \frac{1}{2}$ rule, we obtained the hypertriton lifetime $\tau({}^3_\Lambda\mathrm{H}) = 179(20)$ ps $\approx 0.7(1)\,\tau_\Lambda$.

(5) *Magnitude of theoretical nuclear and hypernuclear structure uncertainties.* The combined spread of Λ separation energies resulting from variation of the $(\Lambda_{NN}, T_{\mathrm{Lab}}^{\max}, \Lambda_{YN})$ χEFT interaction cutoffs is found to be $90 \lesssim B_\Lambda \lesssim 190$ keV, while the spread in calculated two-body π^- rates $1.0 \lesssim \Gamma({}^3_\Lambda\mathrm{H} \to {}^3\mathrm{He} + \pi^-) \lesssim 1.4$ GHz. This implies $160(20) \lesssim \tau({}^3_\Lambda\mathrm{H}) \lesssim 230(30)$ ps for $R_3 = 0.35(4)$.

(6) *Comparison with recent RHI measurements.* The lifetime $\tau({}^3_\Lambda\mathrm{H})$ varies strongly with B_Λ. It is then not possible to exclude any of the distinct RHI $\tau({}^3_\Lambda\mathrm{H})$ measured values, but rather relate the lifetime with its own underlying value of B_Λ. We note the good agreement between the very recent ALICE measured lifetime value $\tau^{\mathrm{ALICE}}({}^3_\Lambda\mathrm{H}) = 253(11)(6)$ ps associated with the ALICE measured B_Λ value $B_\Lambda^{\mathrm{ALICE}} = 102(63)(67)$ keV [8] and the lifetime value $\tau({}^3_\Lambda\mathrm{H}) = 242(28)$ ps computed at the lowest value $B_\Lambda = 66$ keV reached by us. Nevertheless, only future experiments expected at MAMI, JLab, J-PARC, and CERN will hopefully pin down B_Λ with a better precision than 50 keV and lead to a resolution of the ${}^3_\Lambda$H lifetime puzzle.

ACKNOWLEDGMENTS

We are grateful to Petr Navrátil for helpful advice on extending the nuclear NCSM codes to hypernuclei; to Johann Haidenbauer and Andreas Nogga for providing us with the input LO Bonn-Jülich YN potential; and to Andreas Ekström for providing us the $\mathrm{NNLO_{sim}}$ $NN + NNN$ potentials used in the present work. We also thank Assumpta Parreño and Àngels Ramos for valuable discussions. This work was supported by the European Union's Horizon 2020 research and innovation program under Grant Agreement No. 824093 (E.F., A.G., and D.G.); by the Czech Science Foundation GAČR Grant No. 22-14497S (D.G.); and by Secretaria d'Universitats i Recerca del Departament d'Empresa i Coneixement de la Generalitat de Catalunya, cofunded by the European Union Regional Development Fund within the ERDF Operational Program of Catalunya (project QuantumCat, ref. 001-P-001644) (A.P.-O.). Some of the computational resources were supplied by IT4Innovations Czech National Supercomputing Center supported by the Ministry of Education, Youth and Sports of the Czech Republic through the e-INFRA CZ (ID:90140).

APPENDIX A: WEAK-DECAY OPERATOR MATRIX ELEMENTS

In order to evaluate the matrix element of the transition operator (10) in Eq. (6) between the nuclear, hypernuclear (18), and pionic (12) wave functions we proceed by decoupling the spin and isospin states as

$$
\begin{aligned}
&\left\langle \Psi_{{}^3\mathrm{He}}\,\phi_\pi \left| \hat{O} \right| \Psi_{{}^3_\Lambda\mathrm{H}} \right\rangle \\
&= \sum_{\alpha'} \int \mathrm{d}p'_{12}\, {p'_{12}}^2\, \mathrm{d}p'_3\, {p'_3}^2 \psi_{\alpha'}(p'_{12}, p'_3) \sum_{\alpha} \sum_{m_{j_{12}}, m'_{l_3}, m_{l_3}} \delta_{l_{12}l'_{12}} \delta_{s_{12}s'_{12}} \delta_{j_{12}j'_{12}} \delta_{m_{j_{12}}m'_{j_{12}}} \delta_{M'M} \delta_{m_{s_3}m'_{s_3}} C^{M'-m_{j_{12}};M'}_{j_{12},j'_3;J',m_{j_{12}}} C^{M-m_{j_{12}};M}_{j_{12},j_3;J,m_{j_{12}}} \\
&\times C^{M'-m_{j_{12}}-m'_{l_3};M'-m_{j_{12}}}_{l'_3,s'_3;j'_3,m'_{l_3}} C^{M-m_{j_{12}}-m_{l_3};M-m_{j_{12}}}_{l_3,s_3;j_3,m_{l_3}} \sqrt{2}\, G_F m_\pi^2 \left[\left(\mathcal{A}_\Lambda + \frac{\mathcal{B}_\Lambda\, q_\pi}{2\overline{M}_{\Lambda N}} (-1)^{m'_{s_3}-\frac{1}{2}} \right) \delta_{t_3 0} + \frac{1}{2} \mathcal{A}_{\Sigma^- n\pi^-} \delta_{t_3 1} \right] \\
&\times \int \mathrm{d}p_3\, p_3^2\, \psi_\alpha(p'_{12}, p_3)\, r^{-3} \sum_{l_\pi} \int \mathrm{d}\hat{p}'_3\, \mathrm{d}\hat{p}_3 Y^*_{l'_3 m'_{l_3}}(\hat{p}'_3) Y_{l_3 m_{l_3}}(\hat{p}_3) Y^*_{l_\pi 0}(\widehat{\vec{p}_3 - \vec{p}'_3})\, \tilde{\phi}_{l_\pi 0}\left(\frac{3}{2} |\vec{p}_3 - \vec{p}'_3| \right),
\end{aligned}
\tag{A1}
$$

where $m_{s_3} = M - m_{j_{12}} - m_{l_3}$, $m'_{s_3} = M' - m'_{j_{12}} - m'_{l_3}$, $C^{m_2;m_3}_{j_1,j_2;j_3,m_1} \equiv \langle j_1 m_1 j_2 m_2 | j_3 m_3 \rangle$ are the CG coefficients, and the spin matrix element was evaluated using

$$
\left\langle m'_{s_3} \left| \vec{\sigma} \cdot q_\pi \hat{z} \right| m_{s_3} \right\rangle = (-1)^{m'_{s_3}-\frac{1}{2}} \delta_{m_{s_3}m'_{s_3}} q_\pi .
$$

The nonprimed and primed quantities are associated with the initial and final states, respectively. Note that we assume the pion momentum $\vec{q}_\pi$ in the $\hat{z}$ direction and the expansion of the pion wave in spherical harmonics has contributions only from $m_\pi = 0$. Consequently, $m_{l_3} = m_{l'_3}$ and the matrix element only depends on the difference of azimuthal angles $\theta_{p_3} - \theta_{p'_3}$ of $\hat{p}_3$ and $\hat{p}'_3$. We

can integrate out one of them, for example by fixing $\theta_{p_3} = 0$ and replacing

$$\int \mathrm{d}\hat{p}'_3 \to 2\pi \int \mathrm{d}\cos\theta_{p'_3}. \tag{A2}$$

The matrix element (A1) simplifies considerably when the π^- wave function is approximated by a PW, $\tilde{\phi}_{\pi;\vec{q}_\pi}(\vec{k}) = \langle \vec{k}|q_\pi \hat{z}\rangle = 1/k^2\delta^{(3)}(\vec{k} - q_\pi\hat{z})$. In this case, the matrix element evaluates to

$$\begin{aligned}\left\langle \Psi_{^3_\Lambda\mathrm{He}}\,\phi_\pi \mid \hat{O} \mid \Psi_{^3_\Lambda\mathrm{H}}\right\rangle = \sum_{\alpha'} \int \mathrm{d}p'_{12}\, {p'_{12}}^2\, \mathrm{d}p'_3\, {p'_3}^2\, \psi'_\alpha(p'_{12}, p'_3) \sum_{\alpha} \sum_{m_{j_{12}}, m_{l_3}} \delta_{l_{12}l'_{12}}\delta_{s_{12}s'_{12}}\delta_{j_{12}j'_{12}}\delta_{m_{j_{12}}m'_{j_{12}}}\delta_{M',M}\delta_{m_{s_3}m'_{s_3}}\delta_{m_{l_3}m'_{l_3}} C^{M'-m_{j_{12}};M'}_{j_{12},j'_3;J',m_{j_{12}}} \\ \times C^{M-m_{j_{12}};M}_{j_{12},j_3;J,m_{j_{12}}} C^{M'-m_{j_{12}}-m'_{l_3};M'-m_{j_{12}}}_{l'_3,s'_3;j'_3,m'_{l_3}} C^{M-m_{j_{12}}-m_{l_3};M-m_{j_{12}}}_{l_3,s_3;j_3,m_{l_3}} \sqrt{2}\, G_F m_\pi^2 \Bigg[\left(\mathcal{A}_\Lambda + \frac{\mathcal{B}_\Lambda\, q_\pi}{2\overline{M}_{\Lambda N}}(-1)^{m'_{s_3}-\frac{1}{2}}\right)\delta_{t_3 0} \\ + \frac{1}{2}\mathcal{A}_{\Sigma^- n\pi^-}\delta_{t_3 1}\Bigg] 2\pi \int \mathrm{d}\cos\theta_{p'_3}\, Y^*_{l'_3 m'_{l_3}}(\hat{p}'_3) Y_{l_3 m_{l_3}}\left(\widehat{\vec{p}_3\,' + \frac{2}{3}q_\pi\hat{z}}\right) \psi_\alpha\left(p'_{12}, \left|\vec{p}_3\,' + \frac{2}{3}\,q_\pi\hat{z}\right|\right),\end{aligned} \tag{A3}$$

where the nonprimed and primed quantities are again associated with the initial and final states, respectively. Here, the azimuthal part of $\hat{p}'_3$ has been fixed to zero since there is no dependence on it and the factor 2π comes from the replacement (A2).

APPENDIX B: FOURIER TRANSFORM OF THE DISTORTED π^- WAVE FUNCTION

The distorted pion wave function is typically obtained by solving Schrödinger or Klein-Gordon equation with π^--nuclear optical potentials in position space. The momentum-space representation, entering the matrix element in Eq. (5), is obtained by its Fourier transform.

For a function expanded in spherical harmonics $Y_{lm}(\hat{r})$ as

$$f(\vec{r}) = \sum_{l,m} R_{lm}(r) Y_{lm}(\hat{r}), \tag{B1}$$

where the coefficients $R_{lm}(r)$ contain its radial dependence, we define the Fourier transform by

$$\begin{aligned}\mathcal{F}[f(\vec{r})](\vec{k}) &\equiv \frac{1}{(2\pi)^3}\int \mathrm{d}^3 r\, e^{-i\vec{k}\cdot\vec{r}} f(\vec{r}) \\ &= \frac{1}{2\pi^2}\sum_{l,m}(-i)^l Y_{lm}(\hat{k}) \int_0^\infty \mathrm{d}r r^2 j_l(kr) R_{lm}(r).\end{aligned} \tag{B2}$$

Here, the exponential function was expanded in terms of spherical harmonics and spherical Bessel functions $j_l(kr)$ using

$$e^{-i\vec{k}\cdot\vec{r}} = 4\pi \sum_{l,m}(-i)^l j_l(kr) Y^*_{lm}(\hat{k}) Y_{lm}(\hat{r}). \tag{B3}$$

Note that for a π^- PW, $f(\vec{r}) = e^{i\vec{q}_\pi\cdot\vec{r}}$, the coefficient functions in Eq. (B1) become

$$R^{(\mathrm{PW})}_{lm}(r) = 4\pi\, i^l Y^*_{lm}(\hat{q}_\pi) j_l(q_\pi r) \tag{B4}$$

and we recover the momentum-space π^- PW

$$\mathcal{F}[e^{i\vec{q}_\pi\cdot\vec{r}}](\vec{k}) = \frac{1}{k\, q_\pi}\delta(\hat{k} - \hat{q}_\pi)\,\delta(k - q_\pi), \tag{B5}$$

in line with our normalization, $\langle \vec{k}|\vec{q}_\pi\rangle = 1/k^2\,\delta^{(3)}(\vec{k} - \vec{q}_\pi)$. In case of π^- DW, the spherical Bessel functions in Eq. (B4) are replaced by the partial-wave components $\phi_l(q_\pi; r)/(q_\pi\, r)$ of the coordinate-space π^- wave function. The Fourier transform of the DW can be expressed as

$$\mathcal{F}\left[\sum_{l,m} Y_{lm}(\hat{r}) R^{(\mathrm{DW})}_{lm}(r)\right](\vec{k}) = \sum_{l,m} \tilde{\phi}_{lm}(k)\, Y_{lm}(\hat{k}), \tag{B6}$$

where

$$R^{(\mathrm{DW})}_{lm}(r) = 4\pi\, i^l\, Y^*_{lm}(\hat{q}_\pi)\frac{1}{q_\pi\, r}\,\phi_l(q_\pi; r), \tag{B7}$$

and the momentum-space π^- partial waves

$$\tilde{\phi}_{lm}(k) = Y^*_{lm}(\hat{q}_\pi)\frac{2}{\pi\, q_\pi}\int_0^{R_{\max}} \mathrm{d}r\, r\, j_l(kr)\,\phi_l(q_\pi; r) \tag{B8}$$

then enter the matrix elements of the weak-decay operator in Eq. (A1). During evaluation of the matrix elements, the pion momentum is assumed to point in the z direction, $\vec{q}_\pi = q_\pi\hat{z}$, and the spherical harmonic in Eq. (B8) reduces to $Y^*_{l0}(\hat{z})$. Note that a finite value of $R_{\max}$ in Eq. (B8) introduces a certain limit on the momentum scale that $\tilde{\phi}_{lm}(k)$ can probe. The function $\tilde{\phi}_{lm}(k)$ oscillates with frequencies proportional to $R_{\max}$. For example, in the case when $\phi_l(q_\pi; r)$ is a PW and $\tilde{\phi}_{lm}(k)$ is an approximation to $\delta(k - q_\pi)$, the amplitude of these oscillations should be small enough to suppress any structure of the wave functions multiplying $\delta(k - q_\pi)$ in the matrix elements at this scale. In the numerical implementation, the value $R_{\max} = 60$ fm for the upper bound of the integral in Eq. (B8) was found sufficiently large to capture the low-momentum structure of the π^- wave function. On the other hand, the momentum grid used in computing the matrix elements has been chosen fine enough, $\Delta k = 0.0025$ fm^{-1}, such that the oscillations in $\tilde{\phi}_{lm}(k)$ are well resolved. We verified that the calculated decay rates were stable with increasing $R_{\max}$ and decreasing Δk.

[1] A. Gal, E. V. Hungerford, and D. J. Millener, Strangeness in nuclear physics, Rev. Mod. Phys. **88**, 035004 (2016).

[2] H. Le, J. Haidenbauer, U. G. Meißner, and A. Nogga, Separation energies of light Λ hypernuclei and their theoretical uncertainties, Eur. Phys. J. A **60**, **3** (2024).

[3] D. Logoteta, I. Vidana, and I. Bombaci, Impact of chiral hyperonic three-body forces on neutron stars, Eur. Phys. J. A **55**, 207 (2019).

[4] D. Gerstung, N. Kaiser, and W. Weise, Hyperon–nucleon three-body forces and strangeness in neutron stars, Eur. Phys. J. A **56**, 175 (2020).

[5] E. Friedman and A. Gal, Constraints from Λ hypernuclei on the ΛNN content of the Λ-nucleus potential, Phys. Lett. B **837**, 137669 (2023); Λ hypernuclear potentials beyond linear density dependence, Nucl. Phys. A **1039**, 122725 (2023).

[6] P. Eckert, P. Achenbach *et al.*, Chart of hypernuclides – Hypernuclear structure and decay data (2021), https://hypernuclei.kph.uni-mainz.de.

[7] R.L. Workman *et al.* (Particle Data Group), The reviews of particle physics, Prog. Theor. Exp. Phys. **2022**, 083C01 (2022).

[8] S. Acharya *et al.* (ALICE Collaboration), Measurement of the lifetime and Λ separation energy of ${}^{3}_{\Lambda}$H, Phys. Rev. Lett. **131**, 102302 (2023).

[9] L. Adamczyk *et al.* (STAR Collaboration), Measurement of the ${}^{3}_{\Lambda}$H lifetime in Au+Au collisions at the BNL Relativistic Heavy Ion Collider, Phys. Rev. C **97**, 054909 (2018).

[10] C. Rappold *et al.* (HypHI Collaboration), Hypernuclear spectroscopy of products from ^{6}Li projectiles on a carbon target at 2 *A*GeV, Nucl. Phys. A **913**, 170 (2013).

[11] M. Abdallah *et al.* (STAR Collaboration), Measurements of ${}^{3}_{\Lambda}$H and ${}^{4}_{\Lambda}$H lifetimes and yields in Au+Au collisions in the high baryon density region, Phys. Rev. Lett. **128**, 202301 (2022).

[12] *International Conference on Hyperfragments*, St. Cergue, Switzerland, 28–30 March, 1963, edited by W. O. Lock, CERN Yellow Reports: Conference Proceedings (CERN, Geneva, 1964).

[13] R. E. Phillips and J. Schneps, Lifetimes of light hyperfragments. II, Phys. Rev. **180**, 1307 (1969).

[14] G. Keyes *et al.*, New measurement of the ${}_{\Lambda}$H^{3} lifetime, Phys. Rev. Lett. **20**, 819 (1968).

[15] G. Keyes *et al.*, Properties of ${}_{\Lambda}$H^{3}, Phys. Rev. D **1**, 66 (1970).

[16] G. Bohm *et al.*, On the lifetime of the ${}^{3}_{\Lambda}$H hypernucleus, Nucl. Phys. B **16**, 46 (1970); **16**, 523(E) (1970).

[17] G. Keyes, J. Sacton, J. H. Wickens, and M. M. Block, A measurement of the lifetime of the ${}_{\Lambda}$H^{3} hypernucleus, Nucl. Phys. B **67**, 269 (1973).

[18] B. I. Abelev *et al.* (STAR Collaboration), Observation of an antimatter hypernucleus, Science **328**, 58 (2010).

[19] J. Adam *et al.* (ALICE Collaboration), ${}^{3}_{\Lambda}$H and ${}^{3}_{\bar{\Lambda}}\overline{\mathrm{H}}$ production in Pb-Pb collisions at $\sqrt{s_{\mathrm{NN}}} = 2.76$ TeV, Phys. Lett. B **754**, 360 (2016).

[20] S. Acharya *et al.* (ALICE Collaboration), ${}^{3}_{\Lambda}$H and ${}^{3}_{\bar{\Lambda}}\overline{\mathrm{H}}$ lifetime measurement in Pb-Pb collisions at $\sqrt{s_{\mathrm{NN}}} = 5.02$ TeV via two-body decay, Phys. Lett. B **797**, 134905 (2019).

[21] H. Kamada, J. Golak, K. Miyagawa, H. Witala, and W. Glöckle, Pi mesonic decay of the hypertriton, Phys. Rev. C **57**, 1595 (1998).

[22] A. Gal and H. Garcilazo, Towards resolving the ${}^{3}_{\Lambda}$H lifetime puzzle, Phys. Lett. B **791**, 48 (2019).

[23] A. Pérez-Obiol, D. Gazda, E. Friedman, and A. Gal, Revisiting the hypertriton lifetime puzzle, Phys. Lett. B **811**, 135916 (2020).

[24] F. Hildenbrand and H. W. Hammer, Lifetime of the hypertriton, Phys. Rev. C **102**, 064002 (2020).

[25] P. Eckert *et al.*, Systematic treatment of hypernuclear data and application to the hypertriton, Rev. Mex. Fis. Suppl. **3**, 0308069 (2022).

[26] M. Rayet and R. H. Dalitz, Lifetime of ${}_{\Lambda}$H^{3}, Nuovo Cim. A **46**, 786 (1966).

[27] J. G. Congleton, A Simple model of the hypertriton, J. Phys. G **18**, 339 (1992).

[28] P. M. M. Maessen, T. A. Rijken, and J. J. de Swart, Soft core baryon baryon one boson exchange models. II. Hyperon-nucleon potential, Phys. Rev. C **40**, 2226 (1989).

[29] A. Nogga, H. Kamada, and W. Glöeckle, The hypernuclei ${}^{4}_{\Lambda}$He and ${}^{4}_{\Lambda}$H: Challenges for modern hyperon-nucleon forces, Phys. Rev. Lett. **88**, 172501 (2002).

[30] !F. Hildenbrand and H. W. Hammer, Pionic final state interactions and the hypertriton lifetime, Eur. Phys. J. A **59**, 280 (2023).

[31] J. Golak, K. Miyagawa, H. Kamada, H. Witala, W. Glockle, A. Parreno, A. Ramos, and C. Bennhold, The Non-mesonic weak decay of the hypertriton, Phys. Rev. C **55**, 2196 (1997); **56**, 2892(E) (1997).

[32] A. Pérez-Obiol, D. R. Entem, and A. Nogga, $\Lambda N \to NN$ EFT potentials and hypertriton non-mesonic weak decay, J. Phys. Conf. Ser. **1024**, 012033 (2018).

[33] M. Ablikim *et al.* (BESIII Collaboration), Polarization and entanglement in baryon-antibaryon pair production in electron-positron annihilation, Nat. Phys. **15**, 631 (2019).

[34] J. F. Donoghue, E. Golowich, and B. R. Holstein, *Dynamics of the Standard Model* (Cambridge University Press, Cambridge, 2014), Vol. 2.

[35] E. Friedman and A. Gal, In-medium nuclear interactions of low-energy hadrons, Phys. Rep. **452**, 89 (2007).

[36] E. Friedman and A. Gal, Testing in-medium πN dynamics on pionic atoms, Nucl. Phys. A **928**, 128 (2014).

[37] E. Friedman and A. Gal, The pion-nucleon σ term from pionic atoms, Phys. Lett. B **792**, 340 (2019).

[38] E. Friedman (unpublished).

[39] R. A. Arndt, W. J. Briscoe, I. I. Strakovsky, and R. L. Workman, Extended partial-wave analysis of πN scattering data, Phys. Rev. C **74**, 045205 (2006).

[40] E. Friedman *et al.*, The in-medium isovector πN amplitude from low energy pion scattering, Phys. Rev. Lett. **93**, 122302 (2004).

[41] E. Friedman *et al.*, Elastic scattering of low energy pions by nuclei and the in-medium isovector πN amplitude, Phys. Rev. C **72**, 034609 (2005).

[42] B. R. Barrett, P. Navrátil, and J. P. Vary, *Ab initio* no core shell model, Prog. Part. Nucl. Phys. **69**, 131 (2013).

[43] R. Wirth, D. Gazda, P. Navrátil, and R. Roth, Hypernuclear no-core shell model, Phys. Rev. C **97**, 064315 (2018).

[44] P. Navrátil, G. P. Kamuntavicius, and B. R. Barrett, Few nucleon systems in translationally invariant harmonic oscillator basis, Phys. Rev. C **61**, 044001 (2000).

[45] B.D. Carlsson, A. Ekstrom, C. Forssen, D.F. Stromberg, G.R. Jansen, O. Lilja, M. Lindby, B.A. Mattsson, and K. A. Wendt, Uncertainty analysis and order-by-order optimization of chiral nuclear interactions, Phys. Rev. X **6**, 011019 (2016).

[46] H. Polinder, J. Haidenbauer, and U.-G. Meißner, Hyperon-nucleon interactions: A chiral effective field theory approach, Nucl. Phys. A **779**, 244 (2006).

[47] J. Haidenbauer, U.-G. Meißner, A. Nogga, and H. Polinder, *The Hyperon-nucleon interaction: Conventional versus effective field theory approach*, in *Topics in Strangeness Nuclear Physics*, Lecture Notes in Physics (Springer, Berlin, 2007), Vol. 724, p. 113.

[48] T. Y. Htun, D. Gazda, C. Forssén, and Y. Yan, Systematic nuclear uncertainties in the hypertriton system, Few Body Syst. **62**, 94 (2021).

[49] D. Gazda, T. Y. Htun, and C. Forssén, Nuclear physics uncertainties in light hypernuclei, Phys. Rev. C **106**, 054001 (2022).

[50] K. A. Wendt, C. Forssén, T. Papenbrock, and D. Sääf, Infrared length scale and extrapolations for the no-core shell model, Phys. Rev. C **91**, 061301(R) (2015).

[51] C. Forssen, B.D. Carlsson, H.T. Johansson, D. Saaf, A. Bansal, G. Hagen, and T. Papenbrock, Large-scale exact diagonalizations reveal low-momentum scales of nuclei, Phys. Rev. C **97**, 034328 (2018).

[52] S. König, S.K. Bogner, R.J. Furnstahl, S.N. More, and T. Papenbrock, Ultraviolet extrapolations in finite oscillator bases, Phys. Rev. C **90**, 064007 (2014).

[53] J. Adam *et al.* (STAR Collaboration), Measurement of the mass difference and the binding energy of the hypertriton and antihypertriton, Nat. Phys. **16**, 409 (2020).